IMPACTS OF PREDICTED SEA-LEVEL RISE AND EXTREME STORM EVENTS ON THE TRANSPORTATION INFRASTRUCTURE IN THE SAN FRANCISCO BAY REGION

A White Paper from the California Energy Commission's California Climate Change Center

Prepared for: California Energy Commission

Prepared by: University of California, Berkeley

JULY 2012

CEC-500-2012-040

Greg S. Biging

Professor, University of California, Berkeley
College of Natural Resources

John D. Radke

Associate Professor, University of California, Berkeley
College of Environmental Design

Jun Hak Lee

Post Doctoral Fellow, University of California, Berkeley
College of Natural Resources

ACKNOWLEDGEMENTS

We would like to thank the many reviewers (not all known to us) of this work, which includes researchers from California state agencies and universities, Caltrans, Bay Conservation and Development Commission, Alameda County Flood Control & Water Conservation District, University of California, San Diego Scripps, and University of California, Berkeley. Reviewers include Dr. Dan Cayan, Wendy Goodfriend, Tim Doherty, Dr. Peng Gong, Dr. Koohong Chung, Garth Hopkins and Vahid Nowshiravan. Thanks to Wendy Goodfriend for helping us obtain the LiDAR data in an expedient manner and also for providing numerous contacts in these agencies. We thank Dr. Noah Knowles for providing a key input layer necessary for our analysis and Dr. Dan Cayan and Dr. Peter Bromirski for their counsel on sea-level rise and extreme storm events. Dr. Michael Hanemann deserves special acknowledgment for providing insight and guidance in forming some of the key questions that we addressed. Guido Franco has been critical in providing the vision for this work as well as for the entire Public Interest Energy Research Program project. This research work is made stronger by their collective input and we are grateful to them for sharing their expertise with us. Any mistake in this research document is the responsibility of the authors alone.

ABSTRACT

Literature concerning the potential effect of climate change (sea-level rise inundation and 100-year storm events) on the San Francisco Bay region's transportation infrastructure is reviewed. Currently available geographical information system data is employed, and a review of how those datasets have been used in previous studies is reported. The second part of this paper presents methods. They include a higher-resolution digital elevation model for the Bay Area; a new approach using a digital surface model is introduced to improve the surface elevations of features and better calculate the risk of over-topping by sea level shifts and storm surges. A metric to assess change in the transportation infrastructure is introduced that calculates accessibility of first responders to the population at large. Sea level rise is incremented to the expected 1.4 meters in tandem with a 100-year flood to analyze the extent to which transportation assets are at risk of inundation.

The increased travel time from first responder locations to all neighborhoods in the region is measured for each iteration of the model. Local accessibility analysis for the entire San Francisco Bay region is performed to provide a synoptic view. Two localities are chosen to view in detail the impact on first-responder accessibility caused by sea level rise and a 100-year storm event. Next, the regional vulnerability of the transportation network to these events is assessed. This is accomplished by creating nodes that are the intersections of the major regional highways that surround the Bay. The loss of accessibility is measured by calculating the changes in travel time between these major nodes through iterations of our inundation model. Finally, the accessibility impacts to the hinterland from the major highway intersections for each peak water level iteration is determined, calculating the first and last 20 minutes of an origin-destination journey.

Keywords: climate change, sea level rise, flooding, inundation, extreme storms, peak water levels, transportation infrastructure vulnerability, ports, airports, roads, accessibility, first responder accessibility, travel time changes, digital elevation model, DEM, digital surface model, DSM, LiDAR, location-allocation.

Please use the following citation for this paper:

Biging, Greg S., John D. Radke, and Jun Hak Lee (University of California, Berkeley). 2012. *Impacts of Predicted Sea-Level Rise and Extreme Storm Events on the Transportation Infrastructure in the San Francisco Bay Region.* California Energy Commission. Publication number: CEC-500-2012-040.

TABLE OF CONTENTS

Acknowledgements ..... **i**

ABSTRACT ..... **ii**

TABLE OF CONTENTS ..... **iii**

LIST OF TABLES ..... **iv**

LIST OF FIGURES ..... **v**

Section 1: Introduction **1**

1.1 Climate Models and Scenarios 4

1.2 Potential Impact of Climate Change Relevant to Transportation 6

Sea-Level Rise and Storm Surge 8

Increased Precipitation 10

Increased Temperature 10

1.3 Vulnerability of the Transportation Network 10

Section 2: Data and Methods **13**

2.1 Potential Inundation 13

Ground Elevation Data (DEM) 13

Comparison of DEM Techniques 17

Digital Surface Model 18

Water Flow Pathways 20

Transportation GIS Data 22

Datums 23

Peak Water Levels 27

2.2 Assessing Vulnerability of the Road Network 28

First Responder Accessibility 28

Node-To-Node Accessibility Impacts on the Major Traffic Corridors 29

Hinterland Accessibility 31

Section 3: Results **32**

3.1 Potential Inundation of Transportation Infrastructure 32

Roads and Rails 32
Ports and Airports 37
The Port of Oakland 41
3.2 Loss of Accessibility by Inundation 44
Loss of Accessibility in Richmond, California 46
Loss of Accessibility in Santa Clara, California 50
3.3 Zonal Vulnerability of the Traffic Network 55
Section 4: Discussion and Conclusions 63
References 65
Glossary 70

LIST OF TABLES

Table 1. Impacts of Climate Change on Transportation 7
Table 2. Definition of Vulnerability in the Literature 11
Table 3. LiDAR Datasets Used for Potential Inundation Analysis (see Dewberry 2011a for USGS accuracy and 2011b for NOAA LiDAR accuracy) 15
Table 4. GIS Data to Study the Impacts of Sea-Level Rise Relevant to Transportation Infrastructure 23
Table 5. Miles of Road at Risk to a 100-Year Extreme Event by County and Type (Highway and Local) Using Water Depth and Water Paths Analysis 33
Table 6. Miles of Road at Risk to a 100-Year Extreme Event by County and Type (Highway and Local) Using Water-Depth Only 34
Table 7. Miles of Rails at Risk to a 100-year Extreme Storm Event by County Using Water Depth and Water Paths Analysis 36
Table 8. Miles of Rails at Risk to a 100-Year Extreme Storm Event by County Using Water Depth-Only Data 37
Table 9. Loss of First Responder Fire Stations in the San Francisco Bay Study Region as a Function of Peak Water Levels 45
Table 10. Area (km^2) in Accessibility Classes in the San Francisco Bay Study Region. Time delay is for additional minutes above the current (normal) commute conditions due to delays caused by peak water levels. 46

LIST OF FIGURES

Figure 1. Projections of Global Mean Sea-Level Rise Using the Surface Air Temperature Simulations from Various GCM Scenarios. The altimetry 3 mm/year trend estimate for global mean SLR is provided in black. 5

Figure 2. Sources of LiDAR Data Available for Studying the Impact of Climate Change on the Transportation Network of the SF Bay Area. California Coastal LiDAR Project - NOAA/USGS SF Bay LiDAR data. The LiDAR data were acquired in 2010–2011. 15

Figure 3. Tiles Used to Compare NOAA-Supplied DEMs and Study-Produced DEMs. The yellow grid represents the North Bay areas for which NOAA supplied LiDAR data and DEMs. Black squares represent the tiles used for the comparison. 17

Figure 4. Percentage of Test Pixels (in 1m x 1m DEM cells) as a Function of Absolute Difference in Elevation (inches). Three test tiles (Figure 3) were used to compare two methods for producing DEMs: NOAA's and the methods reported in this paper. 18

Figure 5. Example of the Difference between Using a DEM and a DSM Near Point Richmond. (a) Image is a DEM, (b) is the inundation area estimated with the DEM that shows the highway as inundated, (c) image is the DSM, and (d) shows the inundation area estimated using the DEM, but the highway elevation comes from the DSM that correctly represents the connectivity of the highway. 20

Figure 6. An Example of the Difference Between Inundation Estimation Methods. (a) Overview of an example area, (b) before inundation, (c) inundation estimation with water depth only, and (d) inundation estimation with water depth and flow path. 22

Figure 7. Different Tidal Datums at the NOAA Alameda Station 24

Figure 8. Daily Tide Height Prediction in Meters Relative to MLLW at Alameda Naval Air Station 25

Figure 9. An Example of the DEM: San Francisco International Airport. (a) Detailed view of the DEM for SFO, (b) the overview of the area (Google Earth), and (c) an oblique view (Google Earth) of a retaining structure at SFO pointed to in (b). The elevation data set is referenced to NAVD88 vertical datum. 26

Figure 10. A 100-Year Storm Event Peak Water Surface in Raster Format. Water level elevations are in meters above the NAVD88 reference datum. 28

Figure 11. The Nodes and Links of the Major Traffic Corridors in the Region of Potential Inundation Due to Rising Sea Levels 31

Figure 12. Miles Vulnerable to a 100-Year Extreme Event in the San Francisco Bay Area. (a) Highways, (b) local roads. 34

Figure 13. Locations in the San Francisco Bay Area Projected to be Impacted by a 100-Year Extreme Storm Event without and with 1.4 m Sea-Level Rise 38

Figure 14. San Francisco International Airport. The potential inundation with the peak water level 2.4 m above the NAVD88 reference datum. 40

Figure 15. San Francisco International Airport. The potential inundation with the peak water level 2.5 m above the NAVD88 reference datum. 40

Figure 16. The Ratio of SFO and OAK Runway at Risk to a 100-Year Flood Event under Different Sea-Level Rise Values (none or 0 m, 0.5 m, 1.0 m, and 1.4 m) 41

Figure 17. The Port of Oakland. This delineates the area at risk of a 100-year flood event under different sea-level rise elevations (none or 0 m, 0.5 m, 1.0 m, and 1.4 m) in the current study 42

Figure 18. Areas of Inundation at the Port of Oakland, Taken from the USGS CASCaDE Project (http://cascade.wr.usgs.gov/data/Task2b-SFBay/index.shtm) That Has Publicly Available Data Generated by Knowles (2009–2010). This delineates the area at risk of a 100-year flood event under different sea-level rise elevations (none or 0 m, 0.5 m, 1.0 m, and 1.5 m). 42

Figure 19. Roads of the Port of Oakland 43

Figure 20. The Ratio of Areas of the Ports of Oakland, Richmond, and San Francisco at Risk to a 100-Year Flood Event under Different Sea-Level Rise (none or 0 m, 0.5 m, 1.0 m, and 1.4 m). 44

Figure 21. Richmond First Responder Accessibility in Minutes. (a) Under normal conditions, (b) under a 100-year extreme storm event with no sea-level rise, (c) under a 100-year extreme storm event with 0.5 meter sea-level rise, (d) under a 100-year extreme storm event with 1.0 meter sea-level rise), (e) under a 100-year extreme storm event with 1.4 meter sea-level rise, and (f) the change in accessibility under a 100-year extreme storm event with 1.4 m sea-level rise relative to normal conditions. 50

Figure 22. Santa Clara First Responder Accessibility. (a) Under a normal conditions, (b) under a 100-year extreme storm event with no sea-level rise, (c) under a 100-year extreme storm event with a 0.5 m sea-level rise, (d) under a 100-year extreme storm event with a 1.0 m sea-level rise, and (e) under a 100-year extreme storm event with a 1.4 m sea-level rise. 53

Figure 23. Time Reduction in Accessibility in First Responders under a 100-Year Storm Event in Combination with 1.4 m Sea-Level Rise 54

Figure 24. Increased Travel Time (as Multiples of Normal Travel Time) between Intersections after a 100-Year Extreme Event with Different Sea-Level Rise Scenarios. (An impressionistic graphic, due to the complexly of the connected graph). (a) None or 0 m, (b) 0.5 m, (c) 1.0 m, and (d) 1.4 m. 57

Figure 25. Increased Travel Time (as Multiples of Normal Travel Time) between Near-Neighbor Intersections after a 100-Year Extreme Event with Different Sea-Level Rise Scenarios. (a) None or 0 m, (b) 0.5 m, (c) 1.0 m, and (d) 1.4 m. 58

Figure 26. Annual Average Daily Traffic Between Near-Neighbor Intersections under Current Conditions 59

Figure 27. Traffic Volume–Weighted Increment of Travel Distance (Travel Distance Increments Multiplied by Traffic Volume) Between Nearest-Neighbor Intersections for the 100-Year Extreme Event with Different Sea-Level Rise Scenarios. (a) None or 0 m, (b) 0.5 m, (c) 1.0 m, and (d) 1.4 m. 60

Figure 28. Hinterland Accessibility to Major Traffic Corridor Intersections 61

Figure 29. Impacts on Hinterland Accessibility to Major Traffic Corridor Intersections by a 100-Year Extreme Event with Different Sea-Level Rise Scenarios. (a) None or 0 m, (b) 0.5 m, (c) 1.0 m, and (d) 1.4 m. 62

Figure 30. As Early as 2050, with Sea-Level Rise, the Water Level with a 1-Year Peak Event Could Equal Today's Water Level with 100-Year Peak Event 64

Unless otherwise noted, all tables and figure are provided by the author.

Section 1: Introduction

The nine county San Francisco Bay Area has an economy of almost $300 billion. The Bay Area economy ranks 24th in the world and on a per capita basis, it ranks ahead of all national economies. This region holds a leading position in global trade (Bay Area Council Economic Institute 2008). The Bay Area region has 620 miles of freeways and 800 miles of state highways. This region has 19,000 centerline miles of local roadways, which are owned and maintained by Bay Area cities and counties (MTC and Caltrans - D4 2008). The population of the Bay Area is almost 7.2 million, and residents take more than 21 million trips per day on average weekdays (MTC and Caltrans - D4 2008). In 2007, more than 82 percent of all trips were made by automobile. About 12 percent of all trips were by walking and biking and 5 percent by public transit. Around 488 million trips were taken and over 54 billion miles of travel were logged yearly on the road networks in the region. More than 26 billion miles of travel were conducted on the region's 620-mile freeway network. By 2035, the Bay Area's population is projected to reach 9 million, and MTC (Metropolitan Transportation Commission) predicts the number of trips will increase to 29.1 million each day (MTC 2009; MTC and Caltrans - D4 2008).

According to the Bay Conservation and Development Commission (BCDC), the Bay Area's rail network[1] has over 600 miles of track and moves both freight and passengers (BCDC 2009). Except for the Bay Area Rapid Transit (BART) and San Francisco Municipal Transportation Agency (MUNI), both passenger and freight service use the same tracks, so that the rail systems have a substantial amount of congestion. In addition, over the next 50 years, freight demand is expected to increase up to 350 percent (MTC 2007; BCDC,2009). Leading products handled by the rail system are steel, waste, scrap, petroleum products, crushed stone, and automobiles. The rail network connects multiple transportation sectors in the Bay Area. For example, the Ports of Richmond and Oakland heavily rely on rail to transport cargo containers. Passenger service connects the major work places in San Francisco, Oakland, and San Jose with other Bay Area cities and inland cities in the Central Valley (Sacramento and Stockton). BART is a critical component of the passenger rail network, providing commuter service in the region (BCDC 2009).

There are three international airports (San Francisco International Airport (SFO), Oakland International Airport (OAK), and San Jose International Airport (SJC)) in the Bay Area. The three airports processed around 60.6 million passengers and 1,451 thousand tons of cargo in 2007 (MTC and Caltrans - D4 2008). However, the long-term trend in air travel in the Bay Area has been reduced because of terrorist attacks in 2001, a national economic recession, and other factors (MTC, BCDC and ABAG 2011). Total Bay Area airport passengers are projected to number between 88–129 million in 2034. Air cargo volume has declined since 2000 reflecting the maturing of the air cargo business. Price competition from trucking and maritime shipping,

[1] The Santa Clara Valley Transportation Authority (VTA) also has a light rail system in the Bay Area. However, VTA is not included.

among other factors, has reduced the overall level of air cargo shipment in the Bay Area by about 4 percent between 2000 and 2007 (MTC, BCDC and ABAG 2011).

The four major ports (Oakland, San Francisco, Redwood City, and Richmond) processed nearly 2,388 thousand twenty-foot equivalents (TEUs) of marine cargo and 29.4 million tons of bulk cargo in the region in 2007. The port of Oakland hosts the largest volume of cargo within the region (it is the nation's fourth busiest port) and carries more exports cargo than imports (MTC and Caltrans - D4 2008). Airports and sea ports are gateways to the rest of the country and the world and generate a significant amount of connected ground transit by cars, trucks, and rails.

Because infrastructure life-span is relatively long, transportation infrastructure is designed to perform under various natural conditions and within a specified range of extreme events. Due to the longevity of transportation infrastructure, current designs and decisions being made now will continuously affect our society during the life-span of these infrastructures. Accordingly, inappropriate decisions made today may lead to additional spending for retrofitting existing infrastructure or repair of serious system failures in the near and distant future (Kahrl and Roland-Holst 2008).

Although many uncertainties exist regarding the consequences of climate change, there is broad scientific agreement that global climate change is occurring and poses important challenges to our environment (Wilkinson et al. 2002). Increases in average mean temperatures, the number of warm days over mid- and high-latitude land areas, and precipitation and temperature extremes are projected to occur with a high degree of confidence. These changes will bring about melting of sea ice and glaciers at high northern latitudes, a warmer and expanded body of ocean water, sea-level rise, and greater flooding and higher storm surges along coastal areas (Intergovernmental Panel on Climate Change [IPCC] 2007; Transportation Research Board 2008).

Transportation professionals are considering climate-related factors in their planning and design of transportation systems (Transportation Research Board 2008). Therefore, it is natural to incorporate the impact of climate change into planning, design, and maintenance of transportation infrastructure, so that vital transportation systems will not fail under expected climate change scenarios. In addition, many decisions made today regarding transportation infrastructure affect the shape of development patterns and land use in the future. Therefore, it is critical that we project future climate change and understand the impact of climate change on transportation infrastructure.

In general, most studies related to climate change impacts on transportation infrastructure have focused on assessing and mapping the direct impact and failure of flooded sections of transportation networks, transshipment facilities (i.e., ports), or origin and destination depots (i.e., airports). However, fewer studies have explored the negative consequences for society and individuals due to the climate-related disruptions that are expected to occur more frequently. A major reason for the lack of these kinds of studies is the difficulty of converting physical damage to some other quantitative metric representing socio-economic damage. For this perspective, vulnerability analysis of transportation networks may be useful because

vulnerability analysis can provide quantitative measures of the social and economic consequences of disruption.

In this study, we first summarize previously conducted studies relevant to the impact of climate change on transportation systems in general. Although we are mainly focused on the vulnerability assessments of transportation infrastructure from potential inundation (due to sea-level rise) in the Bay Area, we review a broader range of literature related to the impact of climate change on transportation infrastructure. Then, we conduct background research for vulnerability analysis on transportation infrastructure and climate change. In order to conduct the vulnerability assessment of the transportation infrastructure of the San Francisco Bay Area, we first transformed recently acquired Light Detection and Ranging (LiDAR) data for the Bay Area into models of ground elevation and models of surface elevation for roads, bridges, buildings, and other infrastructure. These higher resolution elevation and surface models are essential for accurately estimating potential inundation regions. We also created an up-to-date geographic information system (GIS) for the greater Bay Area. It includes important transportation-related GIS data, such as roads, airports, fire stations and hospitals, which are used in studying the effect of climate change on sea-level rise, as well as inundation due to severe storm events on the transportation network.

The research objectives of this study follow:

- Update an older digital elevation model (DEM)–based LiDAR study with a new, more densely sampled, and more accurate dataset.
- Introduce a digital surface model (DSM) to measure additional information about the surface elevations of objects on the ground and produce a more accurate and realistic surface base for flood inundation calculations.
- Examine, assess, and report flood inundation on transportation infrastructures, such as roads, railways, port facilities, airports, and other key facilities. We calculate peak water level (PWL) modeling estimates based on work by Heberger et al. (2009) where PWL = sea-level rise + a 100-year flood event. We assume climate change models are accurate and adopt a mean sea level (MSL) rise of 1.4 meters by the year 2100. We assume Knowles' (2009) output from his TRIM-2D hydrodynamic modeling is correct and adopt it as our 100-year flood event water levels. We do not examine the dozen or so ways in which levees can fail with or without storm surges as this falls outside the scope of this research. We do assume that overtopping, one of the most serious causes of levee failure, leads to inundation and infrastructure failure and renders roads inoperable.
- Introduce local metrics that map the horizontal impact on accessibility caused by disruptions of the transportation infrastructure system due to inundations. These metrics are applied to a series of origin and destination scenarios where we measure the impact of inundation on accessibility. Although we choose access of first responders to local households here (since local governments attempt to plan and design evenly distributed first responder access to citizens that results in a relatively uniform

distribution of local origin-destinations), the process is universal and could be used to study altered access to all assets of interest.

- Measure node-to-node accessibility impacts on the major road traffic corridors and report travel time shifts between the major intersections, as these are the key nodes in the regional traffic infrastructure.
- Model accessibility impacts to the hinterland from the major highway intersections for each peak water level iteration, calculating the first and last 20 minutes of an origin-destination journey

1.1 Climate Models and Scenarios

In order to conduct viable assessments of the impact of climate change on transportation infrastructure, we need to include projections of relevant weather or climate parameters. These projections can be acquired based on our knowledge and understanding of our climate systems. The current understanding of the governing physical and chemical laws controlling the atmosphere-ocean-land systems that comprise earth's climate is quantified and coded in the form of a linked set of finite difference equations. The models, usually formulated in time-dependent fashion, are typically calculated over grid cells of 100–200 km horizontal distance, so by necessity they are approximate and represent many processes that operate on smaller, sub-grid scales using parameterizations. The models are calibrated and validated with historic data sets, and then driven with assumed external forcings, under which they can be used to estimate future climate changes.

Recent studies take advantage of climate projections developed by the Intergovernmental Panel on Climate Change (IPCC) process. Most global or regional scale climate projections are based upon one or more global climate models (GCMs) run under a set of greenhouse gas emission and aerosol scenarios, which in the last two IPCC climate change assessments were prescribed by the IPCC Special Report on Emissions Scenarios (SRES; Nakicenovic et al. 2000). Peterson et al. (2008) predicted the nation's climate changes relevant to transportation by using climate models and greenhouse gas emission scenarios. They collected and archived the resulting data from more than 25 models and used them for their assessment. In addition, three emission scenarios from SRES (B1: low emission; A1B: mid-range emission balanced on all energy sources; and A2: high emissions) are used. In a Gulf Coast study (Keim et al. 2008), up to 21 different GCM runs were used with three emission scenarios (B1, A1B, and A2) from SRES.

Global or regional climate models calculate a set of atmospheric, land, and oceanic variables such as temperature, precipitation, winds, ocean temperatures, and currents over coarse spatial scales. While climate change occurs on a global scale, the impacts of climate change on transportation infrastructure will differ depending on the geographic location and physiographic regions of that infrastructure. As a consequence, different parts of the nation have specific regional characteristics. Thus, in many cases, the outputs from the global climate models are applied as input variables for secondary-effect models that describe specific climate events (such as flooding, soil erosion, local sea-level rise, etc.). Because there is currently not a full understanding of the processes that control the melt and calving of grounded ice into the

global ocean, the estimation of sea-level rise is only partially handled in GCMs. Consequently, in many cases, future sea-level rise is calculated using a secondary offline model or set of models. One family of these models, which is employed in this investigation, is the *semi-empirical* technique, as developed by Rahmstorf (2007). The Vermeer and Rahmstorf (2009) scheme for calculating global sea-level rise is used here.

Bromirski et al. (2012) used the Vermeer and Rahmstorf (2009) scheme to estimate MSL from the GCMs annual surface air temperature projections to quantify a set of MSL scenarios to the end of the century. By 2100 levels between 1.2 and 1.6 m were obtained by Bromirski et al. (2012) under the A1B and A2 scenarios for the CCSM GCM (see Figure 1). Somewhat different values of sea-level rise (SLR), though of the same order of magnitude were employed by Heberger et al. 2009. We use 1.4 m (55 inches) at the year 2100 as the central value of the suite of projections found in Bromirski et al. 2012.

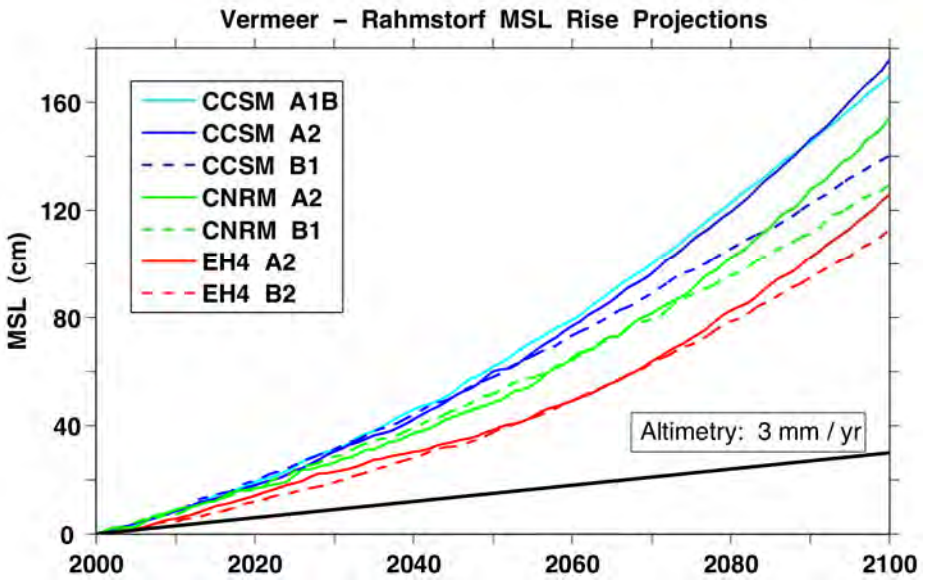

Source: Bromirski et al. (2012)

Figure 1. Projections of Global Mean Sea-Level Rise Using the Surface Air Temperature Simulations from Various GCM Scenarios. The altimetry 3 mm/year trend estimate for global mean SLR is provided in black.

For the San Francisco Bay, a more detailed analysis was conducted (Heberger et al. 2009). Inundation maps were created from the climate change scenarios provided by the U.S. Geological Survey (USGS) (Knowles 2009, 2010). Knowles (2009, 2010) estimated a 100-year projection of MSL rise based on a global climate model (CCSM3) under A2 greenhouse gas emission scenarios for the San Francisco Bay region. Then, to calculate the land surface that is vulnerable to periodic inundation, high water elevation marks throughout the Bay were estimated by using the hydrodynamic model TRIM-2D. Previously calculated SLR estimations from the climate models were then used as a model input to estimate inundation areas. Knowles's work does not account for the effect of wind waves on water levels, land subsidence,

the effect of levees, or fresh water inflows. All of these factors could increase winter flood peaks in estuaries.[2]

1.2 Potential Impact of Climate Change Relevant to Transportation

Transportation infrastructure is designed for typical weather and local climate conditions and is able to function under normal weather fluctuations or within a certain range of weather extremes. As the climate changes, resulting in more extreme and unusual weather patterns, it will cause serious problems for transportation infrastructure. However, no comprehensive inventory exists of the potential impacts of climate change on transportation. The potential impact of climate change on transportation systems can be assessed by the outcomes from the climate models and emission scenarios. Thus, it is convenient to categorize the potential impact by climate parameters (or factors) that are the outcomes of the model predictions.

The general outcomes from the climate models predict an increase in global temperature, changes in precipitation patterns, and SLR. The impact of climate change on transportation has been assessed for a wide variety of purposes and focuses, such as climate factors, geographic regions, and climate zones. For this study, we use key climate parameters to categorize the main impacts of climate change on transportation that are commonly used in the literature. We select four main key climate factors based on both the Transportation Research Board (2008) report and Gulf Coast studies (Keim et al. 2008), and we list the potential impact of climate change on transportation infrastructure. We exclude some key climate factors that are less relevant to the Bay Area's climate conditions (e.g., increases in Arctic temperatures). The selected climate factors are the main outcomes from the climate models and emission scenarios. The main climate factors are SLR, severe storms, temperature, and precipitation. Table 1 lists the effects on weather and climate conditions that are relevant for the transportation sector.

For this study we use Vermeer and Rahmstorf (2009) estimates to make the assumption that MSL rise to the end of the century will reach a level of 1.4 m. Following Cayan et al. (2008), we assume that sea-level rise in the San Francisco outer Bay will closely resemble global mean SLR. This is consistent with the Bromirski et al. (2012) predictions and is the average of the predictive models documented in Figure 1. We assume and use the sea-level rise and 100-year storm events predicted in the literature, but do not include less predictable factors such as Sierra Nevada snow melt.

[2] See Knowles' cited works for additional discussion on limitations of his study.

Table 1. Impacts of Climate Change on Transportation

Climate Impact	Potential Impact	Potential Operational Impact
Sea-level rise and storm surge	Coastal road flooding	Disruption of traffic, delay of evacuation and emergency response, increased congestion. Permanent breaks in the topological structure of the overall transportation network
	Railway flooding	Disruption of traffic, delay, increased risk of hazardous material spill
	Underground tunnels and subway flooding	Disruption and slowdown of subway traffic resulting in increased car, bus, and train commuting
	Erosion of coastal roads and rails	Potential road slump or failure, potential railbed instability or failure
	Port flooding and damage	Negative impact on commerce and manufacturing from delays in cargo handling
	Bridge scour	Erosion of sediment from around bridge abutments or piers, adding to increased maintenance, potential failure, and periodic bridge closures
	Inundation of airport runways in coastal areas	Closure or slowdown in flight arrivals and departures, need for levee construction
	Higher tides at ports facilities	Erosion of shoreline adding to increased maintenance, need for levee construction, and periodic traffic disruption
Severe storms	Damage to facilities at ports	Increased maintenance costs, periodic closures, and transshipment disruptions
	Greater probability of infrastructure failure	Closure or major disruptions and slowdowns in traffic
	Decreased expected lifetime of infrastructure	More frequent and extensive emergency evacuation
Increased precipitation	Overloading of drainage systems, causing infrastructure damage due to flooding	Increases in traffic disruptions and slowdowns
	Damage to infrastructure due to landslides and mudslides	Increased traffic disruptions

Table 1. (continued)

Climate Impact	Potential Impact	Potential Operational Impact
Increased temperature	Highway asphalt rutting	Vehicle overheating and tire deterioration; lane closures for highway repair
	Rail bucking	Increased travel time due to speed restrictions
	Lack of ventilation on underground transit system	Health/safety risks
	Thermal expansion of bridges	Frequent detours

Sea-Level Rise and Storm Surge

A National Research Council report (2008) states that the greatest impact of climate change for the U.S. transportation system will be flooding of roads, railways, the transportation system, and runways around coastal areas (especially along the Gulf and Atlantic Coasts) by the combined effect of sea-level rise and storm surges. Because California has an extensive coastline (approximately 1,100 miles of Pacific coast and 1,000 miles of shoreline along the San Francisco Bay), extreme weather events (such as severe storms or extreme precipitation), especially when exacerbated by sea-level rise will cause the high water levels and have substantial likelihood of being accompanied by sizable wind waves (Cayan et al. 2008). It is assumed that these events would produce the greatest impacts on California's transportation infrastructure (Kahrl and Roland-Holst 2008). Many California coastal areas are at risk from sea level extremes (Flick 1998), especially when sea level extremes are combined with winter storms. For example, very high seas and storm surge caused hundreds of millions of dollars in storm and flood damage in the San Francisco Bay Region in 1997–1998 (Ryan et al. 1999).

In general, streets are lower than the surrounding lands. Water draining from lands adjacent to streets is often drained by flowing into the streets. Thus, streets are the first places to be flooded. Roads in coastal areas will have more frequent flooding by sea-level rise because increased sea level renders the drainage system less effective (Titus 2002). For the entire California coast, Heberger et al. (2009) estimated 3,500 miles of roads will be at inundation risk of a 100-year flood event with a 1.4 m sea-level rise in combination with a 100-year flood as measured above the NAVD88 datum. Under current conditions, only 1,900 miles of coastal roads are at risk of 100-year flooding (detailed climate models and methods were addressed previously). Thus, the length of road at risk of a 100-year flood is almost doubled with a 1.4m sea-level rise compared to the road length at risk of a 100-year flood under current conditions. About half of the roads currently at risk are on the Pacific Coast and the other half (730 miles) are around the San Francisco Bay. A similar estimation was conducted for railways. One hundred and forty miles of railways in California are at risk of 100-year flooding. The length of railways at risk doubles to 280 miles with a 100-year flood event in combination with 1.4 m sea-level rise (above the

NAVD88 datum). About 40 percent of the vulnerable railway lines are around the Pacific Coast and the other parts are in the San Francisco Bay area (68 miles).

The Bay Conservation and Development Commission (BCDC 2009) estimates approximately 99 miles of the major roads and highways are vulnerable to a 16 inch (0.4 m) sea-level rise and approximately 186 miles of the major roads and highways are at risk to a 55 inch (1.4 m) sea-level rise above the average highly monthly (MHW) tide in the Bay Area. Historic tidal data were referenced to find the highest average monthly tide to which sea-level rise estimates were added (Knowles 2008). Furthermore, the BCDC discusses the potential secondary impacts, such as the erosion of existing protective or highway structures from increased storm activities. Another secondary impact is increased congestion caused by more detouring from the impacted roads onto other roads. For the rail network, BCDC estimates approximately 70 miles are vulnerable to sea-level rise of 16-inches (0.4 m) while 105 miles are vulnerable to sea-level rise of 55-inches (1.4 m).

The California Department of Transportation (DOT 2009) also conducted a preliminary assessment of the vulnerability of the transportation system to sea-level rise in California. In their assessment, 350 miles of major streets and highways could be at risk with a 55 inch (1.4 m) sea-level rise by 2100. This study also calculated flooding areas by using topography and the street network in a GIS. However, only highways were included for estimating the impact of inundation. In the California DOT report, the preliminary vulnerability assessment of movement of goods (freight) was conducted and the assessment listed the priority goods movement routes in California affected by a 55 inch (1.4 m) sea-level rise. For the Bay Area, four priority trade route corridors were listed; I-80 in Alameda County, I-880 in Alameda County (from I-80 to US-101), I-80 in San Francisco County, and US-101 in San Francisco County (From I-80 to the San Francisco Airport).

For road and rail networks, as flooding risk increases, a large portion of transportation segments could be blocked by excessive flooding events. As a consequence, more disruption of traffic flow and congestion would be expected. Public transit disruptions by the blocked routes (more likely at underground tunnels or low-lying routes) would cause severe problems for commuters and travelers in the region and additional delays can occur due to increased automobile usage. Furthermore, blocked transportation segments may cause delays in evacuation and emergency response.

While flooding from extreme weather events is temporary, several network links classified as Lifeline Routes are critical to emergency-response and must be repaired and classified operational immediately following a major disaster. Eventually these inundated structures should be permanently repaired in order to make roads and rail networks function correctly, implying time plays a role in infrastructure response from the first flooding to a more permanent restoration. The restoration of infrastructure permanently submerged or even temporarily impacted by a 100-year storm surge may cause additional disruption for longer periods of time and require additional expenses. In addition, San Francisco and Oakland airports will be at risk to flooding, and we anticipate that inundation of runways will interrupt regular operations and cause the closure or delays in flight arrivals and departures.

Naturally, ports are located at the waterfront, and are subsequently exposed to flooding and inundation events. Sea-level rise and storm surge caused by climate change will increase the frequency and magnitude of inundation if ports are not sufficiently protected from these events. Port flooding will have a negative impact on commerce because of delays in processing goods passing through the port. In addition, flooding on the nearby roads and rails could impair or prohibit access to the ports and, hence, the transport of goods and services would be disrupted.

Increased Precipitation

Increased precipitation is likely to cause more frequent overload of the current drainage system. Flooding events could happen not only near the coastlines, but also in inland areas which have insufficient drainage capacity. These events will likely increase the system-wide traffic disruptions and slow down traffic flow. More instances of extreme rainfall will likely contribute to more frequent erosion, tree fall, and landslides, resulting in increased maintenance costs (for both roads and rails). In addition, an increase in frequency of extreme precipitation would increase the rate of traffic accidents, so that the risk of injury and property damage would rise. As weather conditions have a critical influence on airport operations (taking off, landing, and increased traffic separation distances in terminal control areas (TCA) while in flight), extreme rainfall would cause delays due to decreased visibility and wind.

Increased Temperature

The impact of extreme heat on roads could be significant, as it can cause asphalt pavement rutting. Since some pavement materials degrade faster under higher temperature conditions, maintenance cost could increase and require earlier road replacement than anticipated. For rails, higher temperature is dangerous because extreme heat can cause rail bucking, in turn causing critical derailments. Consequently, the speed of transit via trains will likely be reduced under higher temperature conditions and this could cause additional delays on the rail system. Extreme heat may affect the comfort of passengers on public transportation systems. The lack of ventilation systems on underground transportation systems would impact passenger comfort and health. In addition, high temperatures can cause interruptions in electric power distribution due to excessive regional demands for cooling. Power interruptions could lead to delays in public transportation systems that are dependent on electricity (such as BART). As all infrastructure systems are interconnected and most are interdependent, small abnormal events on one system can cause failures of others. In airports, higher temperature reduces the density of air and airplanes at airports consume more fuel and need longer runways to take off. Under these conditions, the current runways may not provide enough length for safe takeoffs, so that closure or slowdown in flight arrivals and departures would be unavoidable.

1.3 Vulnerability of the Transportation Network

In the transportation literature, vulnerability does not yet have a commonly accepted definition, and its meaning may vary for different contexts. In climate change–related literature, the IPCC refers to vulnerability as “The degree to which a system is susceptible to, or unable to cope with, adverse effects of climate change, including climate variability and extremes. Vulnerability is a function of the character, magnitude, and rate of climate variation to which a

system is exposed, its sensitivity, and its adaptive capacity." (IPCC 2001, p. 995) (IPCC Def. 1). Some of the definitions found in the literature are given in Table 2 below.

Table 2. Definition of Vulnerability in the Literature

Authors	Definition of vulnerability
Berdica (2002)	"a susceptibility to incidents that can result in considerable reductions in road network serviceability"
Husdal (2004)	"the non-operability of the network under certain circumstances"
Holmgren, Å . (2004)	"sensitivity to threats and hazards"
Laurentius (1994)	"vulnerability is a susceptibility for rare, though big, risks, while the victims can hardly change the course of events and contribute little or nothing to recovery"
Ford and Smit (2004)	"the susceptibility to harm in a system relative to a stimulus or stimuli"
Nicholls et al. (1999)	"the likelihood of occurrence and impacts of weather and climate related events"
BCDC(2011)	From the Intergovernmental Panel on Climate Change (IPCC 2007): Vulnerability "is the degree to which a system is susceptible to, or unable to cope with, adverse effects of climate change, including climate variability and extremes."

Vulnerability analysis of transportation networks is important because the analysis can provide an insight into their tendency for disruption, the extent of the resulting consequences and the scope of mitigation measures required. Although vulnerability measures have been developed for various disruptions, these measures are also useful in assessing the consequences of climate-related disruption. Regardless of the type of disruption, a reduced level of service of transportation can happen any time.

Despite the significance of the subject, however, it is difficult to characterize network vulnerability because of the complexity and inter-connectivity of the problem. Consequently, the development of a quantitative assessment method is particularly important to manage risks associated with critical events and to compare the benefit and trade-off among various potential responses. Accordingly, several studies have focused on evaluating the vulnerability of the road system in part (or in whole) and determining the most vulnerable elements within the road system itself.

Several studies have focused on assessing the vulnerability of transportation network to natural disasters and climate change. Suarez et al. (2005) analyze the impacts of flooding and climate change on the urban transport system of the Boston Metro Area, applying a four-stage (i.e., trip generation, destination choice, mode choice and route choice) transport modeling system. Sohn (2006) proposed an approach for assessing the significance of highway links in Maryland under flood damage by using an accessibility index. Chang et al. (2010) investigated the potential impact of climate change disruption caused by road closures in the Portland, Oregon. They incorporate climate change scenarios, a hydrologic model, a stream channel survey, a hydraulic model and a travel forecast model to assess the impact of climate change on transportation. BCDC (2011) used a Federal Highway Administration conceptual model for assessing vulnerability and risk of climate change effects on transportation infrastructure from Emeryville to Union City in the San Francisco Bay Area.

An important part of vulnerability analysis is to detect critical components in the network where a certain incident would cause particularly severe consequences. For this purpose, several studies estimate the effect of network degradation through eliminating specific links one at a time and assessing the impact on network operations of the deletion (D'Este 2003; Taylor and D'Este 2004). Taylor et al. (2006) analyze the road network at different levels by using various measures of decreased accessibility to assess the impacts of link failures in Australia. Jenelius et al. (2006) propose an approach for determining the most vulnerable road sections by measuring the link importance indices and site exposure indices of each link. These measures are derived based on the increment of generalized travel cost when links are blocked.

In this literature, accessibility-based consequence measures (increment of generalized cost) are commonly used to assess the vulnerability of road network. Although cutting a single link at a time and incrementing over all links can provide a comprehensive description of the vulnerability of the network, this analysis requires substantial computer power because of the high number of road intersections involved in the calculations. In addition, although it is a good metric of overall vulnerability of the network, it does not measure increased travel time for specific and often critical origin and destination thematic events, such as accessibility of first responders or accessibility to hospitals.

Section 2: Data and Methods

2.1 Potential Inundation

Land surface (elevation) models and peak water levels are the key components needed to accurately estimate potential inundation areas in the San Francisco Bay region. We prepared the land surface models (DEM) by using highly accurate LiDAR data sets.

We follow the methodology of Heberger et al. (2009) for estimating PWLs. Peak water levels have two components: sea-level rise and a 100-year flood event. An important element of a flooding event is that storms coincide with high tides (Zetler et al 1985; Flick 1998).

The 100-year flood is a flood that has a 1/100, i.e., 1 percent chance of occurring per year. It can be shown that there is a 63 percent chance that a 100-year flood will occur over the next 100-year period and a 9.5 percent chance that it will occur over the next 10 years. In this paper we refer to the 100-year flood as a 100-year extreme storm event ((ESE_{100}). Our model has four sea-level rise (SLR_x) increments {x: 0 m, 0.5 m, 1.0 m or 1.4 m} to which we add the 100-year extreme storm event (ESE_{100}) without sea-level rise. Thus our model for peak water level can be written as: $PWL_x = SLR_x + ESE_{100}$. The flood levels (elevation (m)) for the 100-year extreme storm event with no sea-level rise ($PWL_{(0)}$) were provided by Noah Knowles of the USGS, as discussed further in the section Peak Water Levels below.

As pointed out by Heberger et al. (2009),this approach assumes that all tide datums (see the section below on Datums) will increase by the same amount as MSL is projected to increase. It is important to note that San Francisco has the longest continuous tidal record in North America (Bromirski et al. 2003), and when examining tidal datum statistics in the Bay proper, it is observed that mean higher high water (MHHW) rose at 155 mm/century, 92 percent faster than the MSL, and mean high water (MHW) rose at 145 mm/century, 80 percent faster than MSL (Flick et al. 2003). Because of these observations, it is prudent to modify the PWL predictions if the trends observed by Flick et al (2003) continue for extended periods in the future.

Ground Elevation Data (DEM)

We obtained and processed the most accurate, high spatial resolution ground elevation data currently available (see Table 3 and Figure 2). These (LiDAR) data are obtained using an optical remote sensing technology that can measure the distance to a target by illuminating the target with light pulses from a laser (Wehr and Lohr 1999) and are put through a rigorous quality control.[3]

We used two main LiDAR data sets that cover the San Francisco Bay, San Pablo Bay, and Suisun Bay. We obtained the North Bay LiDAR data (that covers areas north of the Bay Bridge) and the South Bay LiDAR data (that cover areas south of the Bay Bridge) from the USGS Center for

[3] See metadata description at:
http://www.csc.noaa.gov/crs/tcm/ldartdat/metatemplate/sfbay2010_template.html

LIDAR Information Coordination and Knowledge (CLICK). The North Bay LiDAR data was collected by Fugro Earth Data, Inc. with a Piper Navajo twin engine aircraft utilizing a Leica ALS60 MPiA 200 kHz LiDAR sensor collecting returns as well as intensity. The South Bay LiDAR was collected by Dewberry with a Piper Navajo twin engine aircraft utilizing an Optech ALTM 3100EA 100 kHz LiDAR sensor collecting returns as well as intensity.

Both data sets were collected as a part of the California Costal LiDAR Project (CCLP). The spatial coverage of the data extends landward 500 m from the shoreline to approximately the 10 m topographic contour. The density of the data is nominally 1 point per 0.7 m^2. Both data sets were provided as a tiled structure (1.5 km by 1.5 km) and LAS 1.2 format (a common LiDAR data exchange format, which was introduced by the American Society of Photogrammetry and Remote Sensing; http://www.lasformat.org). The horizontal spatial reference system for these data sets is the Universal Transverse Mercator projection (NAD83, UTM Zone 10N), and the vertical spatial reference system is the North American Vertical Datum of 1988 (NAVD88).

The accuracy of the USGS LiDAR dataset was assessed by the prime contractor for the LiDAR acquisition campaign (Dewberry 2011a and 2011b). One of the metrics reported is for fundamental vertical accuracy (FVA) which is for the check points located on open terrain. For the USGS San Francisco Coastal LiDAR project, the vertical accuracy was specified to be 18 cm or less. The FVA at the 95 percent confidence level is 0.05 m for the National Oceanic and Atmospheric Administration (NOAA) LiDAR data and 0.12 m for the USGS LiDAR data. The horizontal accuracy is 2.0 m at the 95 percent confidence level for both datasets. So both regions meet and exceed project specifications for vertical accuracy.

We derived a DEM based on these data only after substantial processing of the LiDAR data. We converted the LiDAR point data cloud to raster datasets that provide terrain elevations for ground positions at regularly spaced horizontal intervals. This DEM is used in subsequent analyses. We also developed a DSM and discuss it in the section Digital Surface Model below.

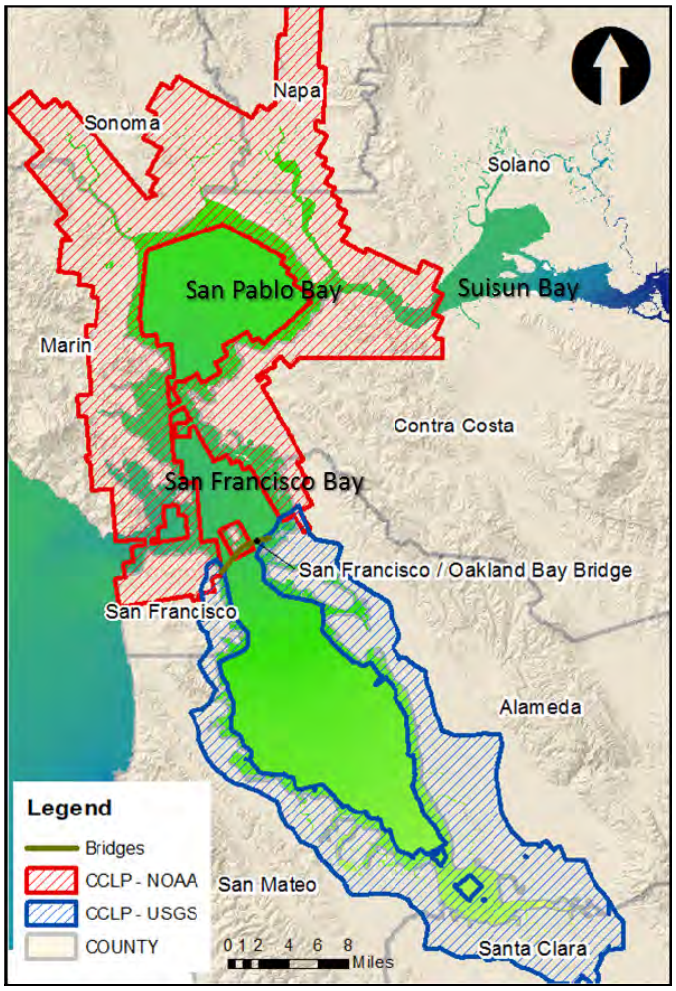

Figure 2. Sources of LiDAR Data Available for Studying the Impact of Climate Change on the Transportation Network of the SF Bay Area. California Coastal LiDAR Project - NOAA/USGS SF Bay LiDAR data. The LiDAR data were acquired in 2010–2011.

Table 3. LiDAR Datasets Used for Potential Inundation Analysis (see Dewberry 2011a for USGS accuracy and 2011b for NOAA LiDAR accuracy)

Name	Projection		Accuracy	
	vertical	Horizontal	Fundamental vertical	Horizontal
NOAA California Coastal LiDAR Project	NAVD88	NAD83, UTM Zone 10N	0.05 meters at 95% confidence level	2.0 meters at 95% confidence level
USGS California Coastal LiDAR Project	NAVD88	NAD83, UTM Zone 10N	0.12 meters at 95% confidence level	2.0 meters at 95% confidence level

For the North Bay data (NOAA region), we obtained both the LiDAR point data and the DEM data so that we did not need to create a DEM for this region. Since the data were provided as a tiled structure, a total of 649 tiles from the DEM dataset were combined into one large file to determine the connectivity to the San Francisco Bay.

For the South Bay data (USGS region), we obtained the LiDAR point data only and therefore had to derive a DEM from them. Because the LiDAR point data contained classification information for each point, we selected certain classes of points, which represent ground surfaces (Class 2 = Ground Class; Class 9 = Water Class). That is, we used all points classified as a ground class. In addition, we included the points that are classified as water to derive the DEM as most of these points were from mudflats (wet ground). The LiDAR sensor uses near-infrared laser pulses. Water bodies absorb near-infrared light and hence do not have any return pulse. Therefore, including the LiDAR points of the water class that are mainly from mud flats or tidal flats is beneficial for generating more accurate and realistic ground elevation data for our study area.

Since the LiDAR point density is sufficiently high, we applied a linear interpolation method to convert the LiDAR point cloud into a DEM. In this procedure, if a single LiDAR point is found in a pixel (1m x 1m), it represents that pixel. If a pixel height is missing, it is interpolated from the surrounding pixels. If multiple LiDAR points exist in a pixel, then the pixel is assigned the highest height observed in that pixel. The interpolation was conducted on a tile-by-tile basis (the original data comprised 712 tiles, each 1.5 km by 1.5 km). If the interpolation is conducted one tile at a time, the edges of each DEM might have some discrepancies between neighboring tiles. In order to cope with this problem and create a seamless DEM data set, we prepared overlapped LiDAR point data sets between the tiles. Accordingly, we produced 1.7 km by 1.7 km tiles that have 100-meter overlap on each shared side between tiles. We conducted a linear interpolation and converted the LiDAR point clouds to a DEM for each tile and clipped out the

DEM to the original tile size (1.5 km by 1.5 km). Finally, we combined all tiled DEMs into one large file to match the North Bay data.

DEMs created with high resolution LiDAR, as done in this study, produce surfaces that are more accurate and with less smoothing than is provided by the National Elevation Dataset (NED) from the USGS. Like our DEM, NED is a raster dataset, but NED has a horizontal resolution of either 30 or 10 m. In NED datasets, small but important objects, like seawalls, levees, bridges and reventments, would not be detected. In our DEM these important objects are both detected and well approximated. The USGS (http://ned.usgs.gov/Ned/accuracy.asp) points out that NED inherits the accuracy of the source DEMs. Likewise, our DEM inherits the accuracy of the source LiDAR used in its creation (see Table 3). This allows us to better predict where low-lying areas might be flooded, overtopped, and isolated from the rest of the land area.

Comparison of DEM Techniques

We selected three tiles, each of size 1500 x 1500 m, to compare the NOAA-supplied DEMs in our northern region (see Figure 3) with DEMs that utilized the same methods to produce DEMs in our southern region. Since the LiDAR point data is already classified into ground and non-ground, we selected only ground points and interpolated by using linear interpolation. We then calculated the difference between these two data sets with each tile comprising 2,250,000 raster values for height.

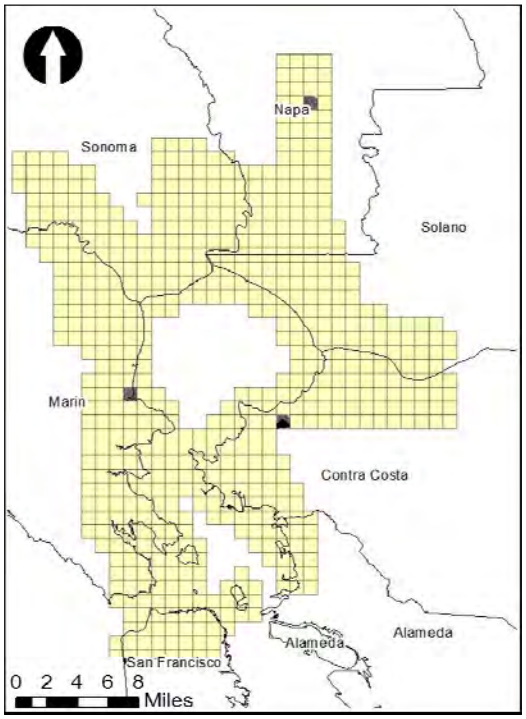

Figure 3. Tiles Used to Compare NOAA-Supplied DEMs and Study-Produced DEMs. The yellow grid represents the North Bay areas for which NOAA supplied LiDAR data and DEMs. Black squares represent the tiles used for the comparison.

We conducted quality control by comparing the pixel height values of the sample tiles to those created using the methods reported in this paper. Figure 4 shows the result of this comparison. More than 63 percent of the raster elevations were within 1.5 inches of each other, and nearly 80 percent were within 2.5 inches. Ninety percent of the elevations were within 5.5 inches of each other. Since our methodology has a high correspondence to that used by NOAA, we applied our DEM methodology to the areas south of the Golden Gate Bridge for which no DEMs had been produced.

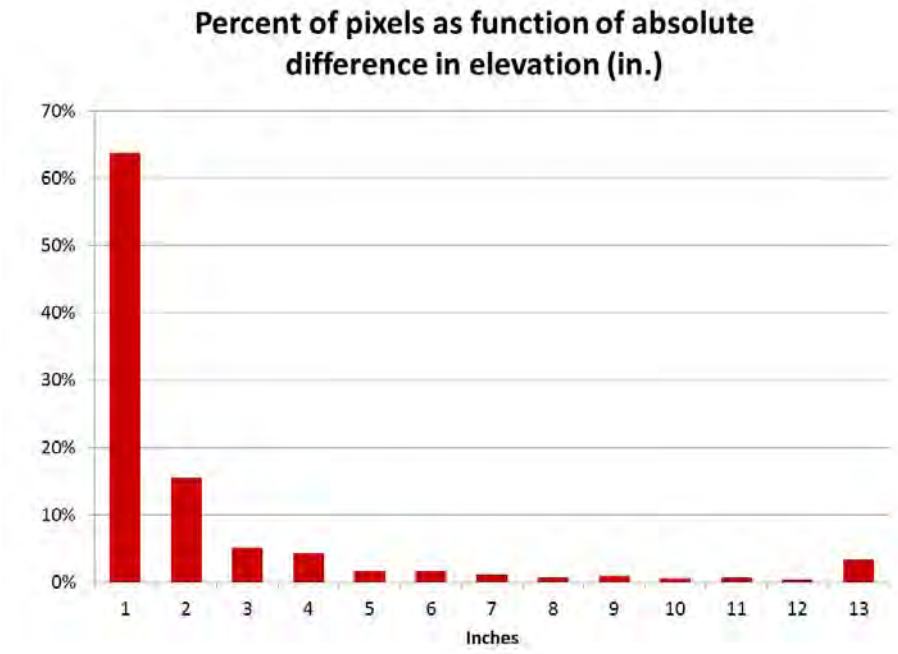

Figure 4. Percentage of Test Pixels (in 1m x 1m DEM cells) as a Function of Absolute Difference in Elevation (inches). Three test tiles (Figure 3) were used to compare two methods for producing DEMs: NOAA's and the methods reported in this paper.

Digital Surface Model

We prepared a digital surface model (DSM) to supplement the DEMs used in our analysis. DSMs contain information about not only the height of bare ground, but also the surface elevations of the objects on the ground (such as buildings, trees, houses, levees). In general, converting LiDAR points to a DEM requires filtering procedures that remove non-ground LiDAR points from the LiDAR point cloud. Although these filtering methods are well developed and in general perform adequately, some transportation objects (such as highways and bridges) may be removed during the LiDAR data filtering procedures used to create a DEM from LiDAR data. In these instances, using only a DEM may result in a false determination of the connectivity of the ground transportation network under a flooding event scenario.

It is common to estimate the potential for inundation of the transportation network using only DEMs with geo-data layers within a GIS (e.g., Heberger et al. 2009; Knowles et al. 2009 and 2010). However, this approach is premised on the assumption that the elevation of transportation features and ground surfaces are the same. In some cases (e.g., local roads) this assumption is convenient and works well. However, in many cases (e.g., raised highways and bridges), the inundation of transportation features are overestimated due to the elevation error imposed by simply mapping ground surfaces. Figure 5(a)-5(d) illustrate an example showing the difference between a DEM and a DSM near the Point Richmond area. Here different surface products can produce differing inundation estimates.

Our method for creating DSMs is similar to that used in the creation of the DEMs. For the DEM we use only points representing ground surface (Class 2 = Ground Class; Class 9 = Water Class). In contrast, we included all classes of LiDAR points, except Class 7 (= Noise Class), to generate the DSM. We conducted the interpolation as we did for creating the DEM on a tile-by-tile basis. In this procedure, if a single LiDAR point is found in a pixel (1m x 1m) it represents that pixel. If a pixel height is missing, it is interpolated from the surrounding pixels. If multiple LiDAR points exist in a pixel, then the pixel is assigned the highest height observed in that pixel. To create seamless raster data, we prepared overlapped point data sets between the tiles. That is, we reproduced 1.7 km by 1.7 km tiles with 100-meter overlap on each side between tiles. We used a linear interpolation algorithm to convert the LiDAR point data into the DSM. Finally, we combined all tiled DSMs into one large file.

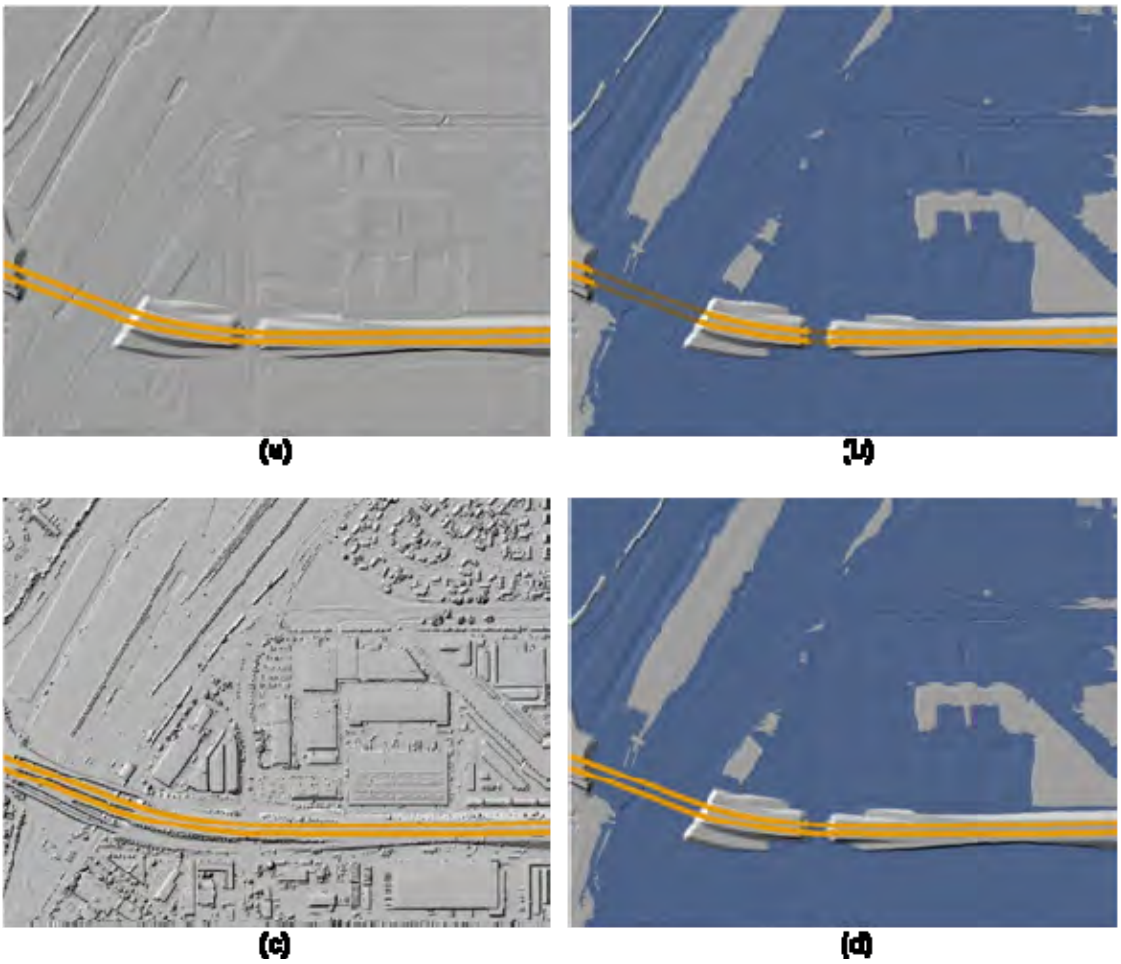

Figure 5. Example of the Difference between Using a DEM and a DSM Near Point Richmond. (a) Image is a DEM, (b) is the inundation area estimated with the DEM that shows the highway as inundated, (c) image is the DSM, and (d) shows the inundation area estimated using the DEM, but the highway elevation comes from the DSM that correctly represents the connectivity of the highway.

Water Flow Pathways

Previous studies, conducted by Heberger et al. (2009) and Knowles et al. (2009, 2010), also used high spatial resolution DEMs (2 m by 2 m horizontal resolution) to determine areas that are potentially flooded by sea-level rise and extreme storm events. However, those studies used water depth alone for estimating areas that would experience flooding. Consequently, some areas may be falsely classified as potential inundation areas because the studies do not consider water pathway, as discussed in the following paragraph, and some areas could be surrounded and thus protected by higher ground or objects such as levees. An example of solely using a DEM and water depth to determine a potential inundation area is illustrated in Figure 6.

In this study, we have sufficiently dense LiDAR coverage (nominally 1 point per 0.7 m^2) to allow us to create 1m x 1m rasters containing elevation point data. This is roughly four times

finer horizontal resolution than used in prior studies having 2m x 2m rasters for elevation point data. This increased horizontal resolution, combined with the high vertical accuracy of these datasets, leads to higher resolution DEMs and DSMs. In addition, we incorporate water flow pathways to improve our ability to estimate flood inundation areas. To do this, we used the connectivity of regions to waters of the San Francisco Bay or Pacific Ocean. The delineation of regions is calculated by using the DSM to obtain the elevations of artifacts, like roadways and levees, to determine whether they are barriers bounding a region or not. The regions that were not connected to water were excluded for the inundation estimation.

First, we compared the ground elevation surface (from the DEM) and the water surface raster. We then select the regions where the ground elevation was lower than the projected peak water level. We analyzed only the regions that are connected to the San Francisco Bay or Pacific Ocean and we removed all other regions that are not connected to these water sources. Hence, the regions that are not connected to the Bay or ocean are excluded from consideration as being in a potential inundation area. The "Region Group" function in ArcGIS was used to determine the connectivity. The function calculates "the identity of the connected region to which that cell belongs" (ESRI 2009). By comparing the elevation of the land and water surface, several regions where the lands are lower than the projected peak water levels were selected. Once selected, each region was assigned with different IDs and each cell in the same region given a same value (a region ID).

We used the DEM to validate region connectivity by eliminating the possibility of discontinuous polygons being hydraulically connected, resulting in valid flow pathways. This is analogous to the method employed by the NOAA Costal Service Center: they used the ArcGIS Spatial Analyst extension and applied similar procedures to account for local/regional tidal variability of mean high higher water for each area. Sea-level rise is added to MHHW. They also use hydrological connectivity to exclude hydrologically unconnected polygons and improve on the bathtub approach to modeling inundation. A description of their methodology can be found at: http://www.csc.noaa.gov/slr/viewer/assets/pdfs/Inundation_Methods.pdf

Figure 6 shows an example of the difference between using *water depth only* and the *water depth and flow path* inundation estimation methods. The *water depth only* method shown in Figure (6c) is based on the DEM only and does not account for the connectivity to the Bay or Pacific Ocean. The inundation estimation mapped in Figure 6d is based on both the DEM and the path that water flows inland over the terrain. Although the inland area is lower than the water level on the outside of the levee, the inland area is not inundated due to the protecting structures or levees. However, high water levels do cause levee stress that can eventually lead to failure, defined as a levee breach. Besides levee overtopping, high water loading functions can produce other failure mechanisms, such as sliding, slump spread, seepage and erosion (Moss and Eller 2007). The probability of levee failures due to high water levels during storm events is estimated to be 0.0579 per year according to the Delta Risk Management Strategy (DRMS) study (URS 2009). Although inundation or repeated inundation could lead to levee failure, failure rate modeling and prediction is outside the scope of this project.

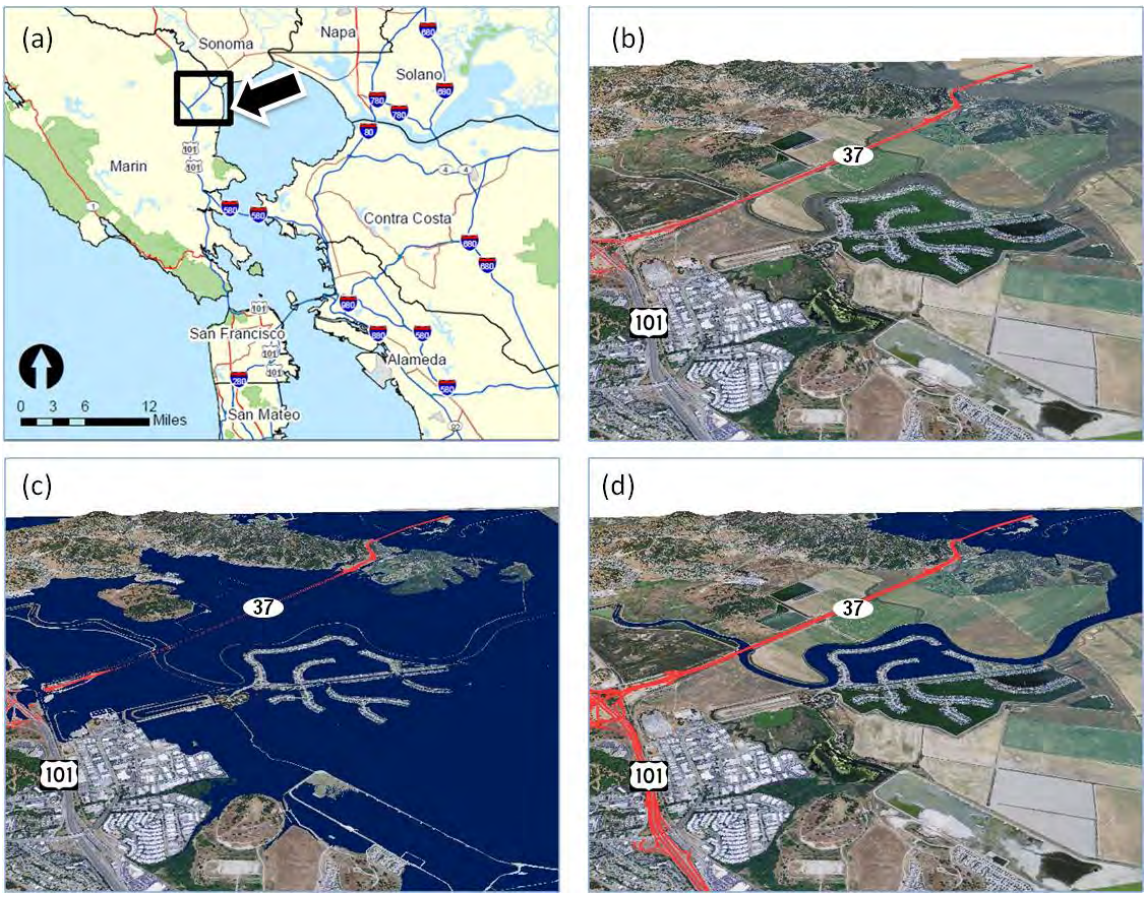

Figure 6. An Example of the Difference Between Inundation Estimation Methods. (a) Overview of an example area, (b) before inundation, (c) inundation estimation with water depth only, and (d) inundation estimation with water depth and flow path.

Transportation GIS Data

In order to conduct quantitative estimation of the impact of sea-level rise on transportation, we need accurate geo-data layers of transportation infrastructure. Various sources provide GIS data sets for different resources (road, rail, airports, ports, etc.).

Table 4 shows currently available GIS data sets relevant for our study on impact analysis. We list the most accurate and up-to-date data sets available. In general, most of these data are publicly available, so that we are able to download and use them directly. However, in some cases, additional processes are needed to improve the quality and usefulness of the data sets. For example, fire station data extracted from the FEMA Hazus (Hazard US) database has a limited number of stations and with outdated information. We employ an address matching algorithm (from the lists of station addresses) to create an accurate data set for fire stations.

Table 4. GIS Data to Study the Impacts of Sea-Level Rise Relevant to Transportation Infrastructure

Categories	Data sources	Notes
Roads	Streetmap Pro (ESRI) (Sept. 2010)	The road network has routing information so that a network analysis is possible
Rails	Streetmap Pro (ESRI)	
BART	MTC	Bay Area Transit database
Airports (Runways)	Streetmap Pro (ESRI)	Transportation database
Healthcare facilities	California Statewide Health Planning and Development	Accessible via Cal-Atlas (http://www.atlas.ca.gov)
Fire stations	Address matching	The locations are geocoded by using Streetmap Pro street network.
Ortho images	National Agriculture Imagery Program (2009)	1 m spatial resolution, RGB, and near infra-red.

Datums

A diagram of the tidal datum elevations at the Alameda Station, Alameda, California, is illustrated in Figure 7. This is a display of the averages for the 1983–2001 epoch. Displayed tidal datums are Mean Higher High Water (MHHW), Mean High Water (MHW), Mean Tide Level (MTL), Mean Sea Level (MSL), Mean Low Water (MLW), and Mean Lower Low Water (MLLW). In brief, MHW is the mean high water which is the average height of all high tides. MHHW is the mean higher high water, which is the average height of the higher of the two daily high tides. MLW is the mean low water, which is the average height of the two daily low tides. For more formal definitions of these and other tidal datums, see Heberger et al. (2009) or go to NOAA's website: http://tidesandcurrents.noaa.gov/datum_options.html.

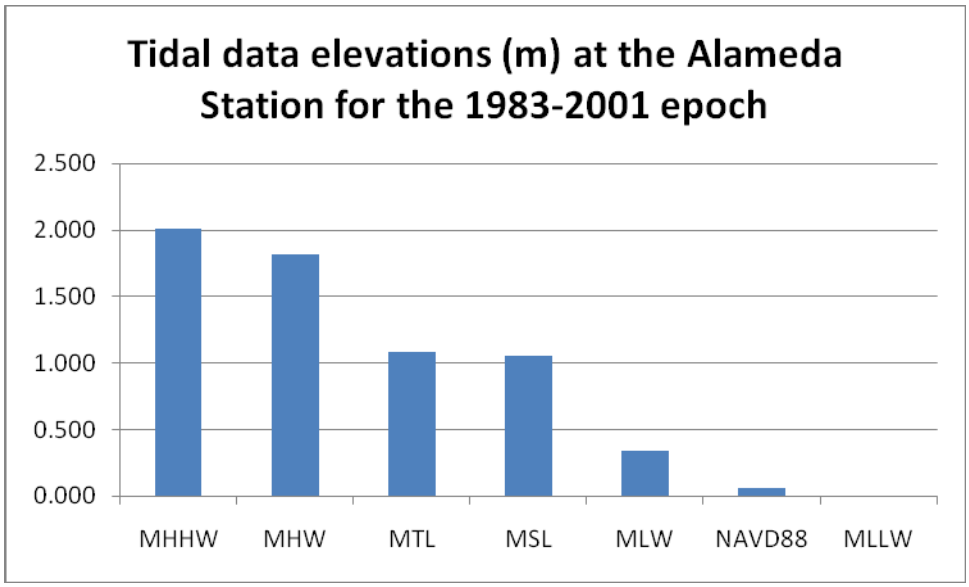

Source: Figure produced by Biging, Radke, and Lee using data from NOAA Tides and Currents (http://tidesandcurrents.noaa.gov/data_menu.shtml?unit=0&format=Apply+Change&stn=9414750+Alameda%2C+CA&type=Datums).

Figure 7. Different Tidal Datums at the NOAA Alameda Station.

Since the San Francisco International Airport (SFO) does not have a tidal station, the Alameda Station (NOAA Station ID: 9414750), being in the proximity of SFO, is used in this example to display tidal and reference datums. MSL is slightly more than 1.0 meter (1.051 m) above the MLLW reference datum, or 0.98 m above the NAVD88 reference datum at Alameda Station averaged over the 1983–2001 epoch. At this location, diurnal tidal heights can vary by over 2 m (see Figure 8).

DEM (and DSM) data are essential for undertaking the rising sea level and 100-year extreme storm inundation analysis on the transportation network of the greater Bay Area. Figure 9a shows a close-up of a DEM produced with our methodology (see the section Ground Elevation Data above) at SFO. In this figure (also refer to Section 3.1 Ports and Airports below and Figure 14), we can see the height of the runways exceeds approximately 3 m above the vertical datum (NAVD88) in this section of the airport. However, in Figures 14 and 15 it can be seen that large portions of the airport are below 2.6 m.

The diurnal tidal heights at Alameda Station can reach approximately 2.0 m above the MLLW datum, as evidenced from the 8/19/2010 daily tide predictions (Figure 8). The tide predictions from this NOAA Tides & Currents website can be projected into the future or back into the past for two calendar years only. The MHHW for the Alameda location is 2.01 m above MLLW, or 1.95 m above NAVD88, for the 1983–2001 epoch (see: http://www.ngs.noaa.gov/newsys-cgi-bin/ngs_opsd.prl?PID=HT0890&EPOCH=1983-2001). Thus, if sea level rise reaches 1 m over present mean sea level, SFO would be overtopped on occasions when astronomical tides reach 2 m. However, sea level actually exceeds high tides on occasions when storm effects elevate sea levels. As discussed more fully in section 3.1 Ports and airports below, this critical facility could

be overtopped if mean sea levels rises 0.5 m, when a 100-year storm event coincides with high astronomical tides.

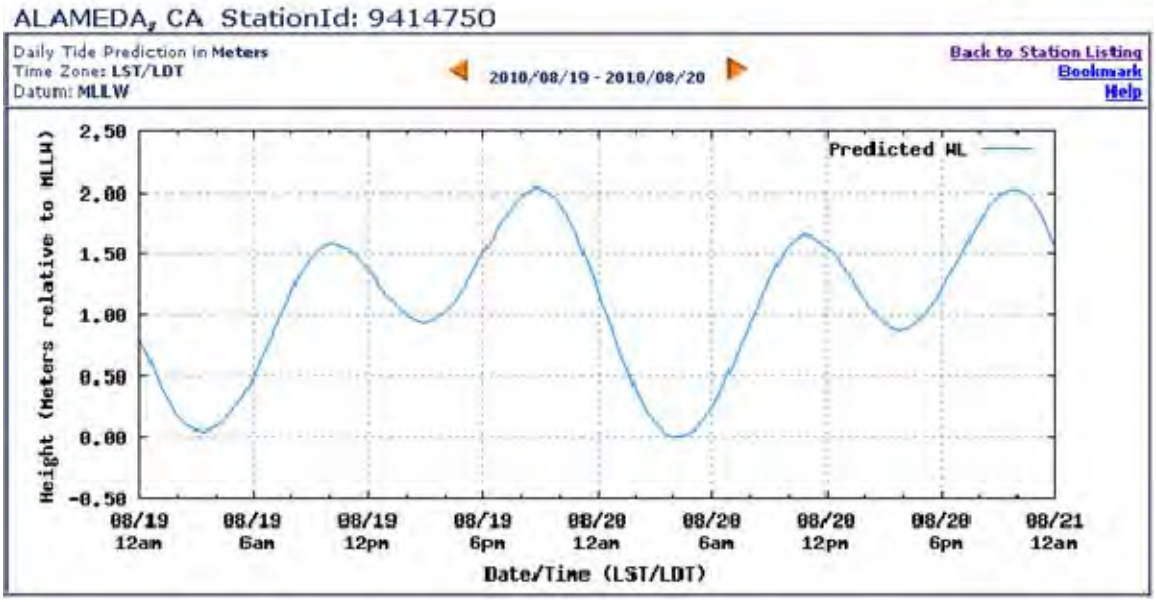

Source: NOAA Tides and Currents
http://tidesandcurrents.noaa.gov/noaatidepredictions/NOAATidesFacade.jsp?Stationid=9414767

Figure 8. Daily Tide Height Prediction in Meters Relative to MLLW at Alameda Naval Air Station.

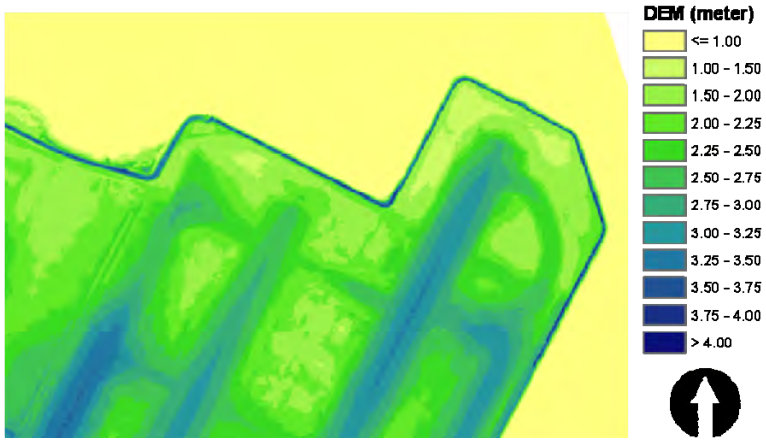

(a)

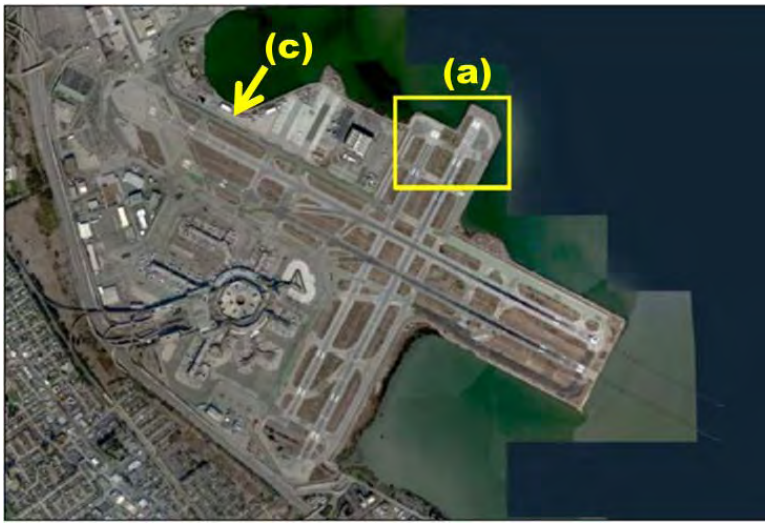

Source: Google Earth (b)

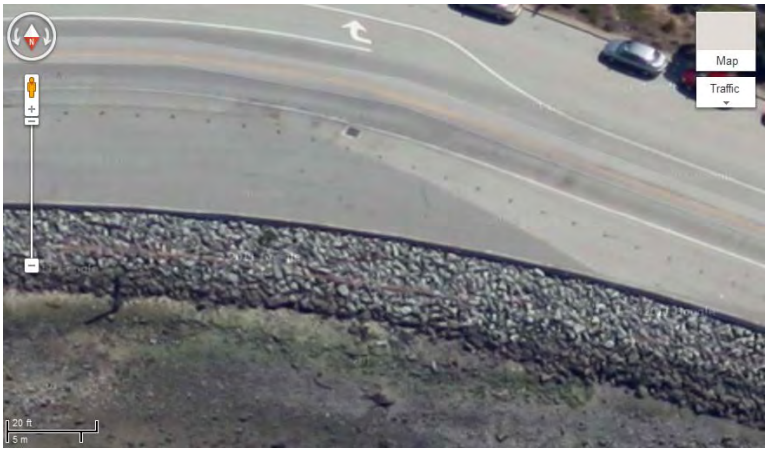

Source: Google Earth (c)

Figure 9. An Example of the DEM: San Francisco International Airport. (a) Detailed view of the DEM for SFO, (b) the overview of the area (Google Earth), and (c) an oblique view (Google Earth) of a retaining structure at SFO pointed to in (b). The elevation data set is referenced to NAVD88 vertical datum.

Peak Water Levels

As pointed out in section 2.1 Potential inundation, land surface (elevation) models and peak water levels are the key components needed to estimate accurate potential inundation areas in the San Francisco Bay region. As stated earlier, our model has four sea-level rise (SLR_x) increments {x: 0 m, 0.5 m, 1.0 m or 1.4 m} to which we add the 100-year extreme storm event (ESE_{100}) without sea-level rise. Thus, peak water level is: $PWL_x = SLR_x + ESE_{100}$. The upper sea-level rise value of 1.4 m corresponds to the mean projection in year 2100 of sea-level rise under the climate models examined (Figure 1).[4]

Knowles (2009) used the TRIM-2D hydrodynamic model and historic variability based on long term gauge readings to model hourly water levels throughout the Bay over 100 years as measured from the NAVD88 datum.[5] Based on a 100-year projection of high water levels (with and without sea-level rise), he determined the high water levels which corresponded to the 100-year return interval. This data was provided by Dr. Knowles (USGS) to this project as a raster of 100 m horizontal resolution (Figure 10). This provides the water levels associated with a 100-year storm which, in our parlance, is the 100-year extreme storm event (ESE_{100}). This high water surface elevation is also used by Heberger et al. (2009). While the water levels are continuous, for interpretation purposes, they were placed into discrete classes to make it easier to read the water heights at the airports and other locations.

It is important to point out that we do not project localized rainfall, nor do we incorporate wave runup, wind-driven waves, or river stage forecasts into our model for peak water levels. These and other factors will cause variations in the PWLs that may lead to localized flooding. It should be clear that our predictions are approximations to a complex hydrodynamic system, and inferences should be tempered by this fact.

---

[4] Knowles (2009, 2010) uses an upper value of 1.5 m. So for his work, the maximum peak water level is $PWL_{(1.5)}$.

[5] We are able to compare the elevation of water and land surfaces (from geo-registered LiDAR data) without any conversion, since Knowles' 100-year flood elevations were measured from the same datum (NAVD88) as the LiDAR data.

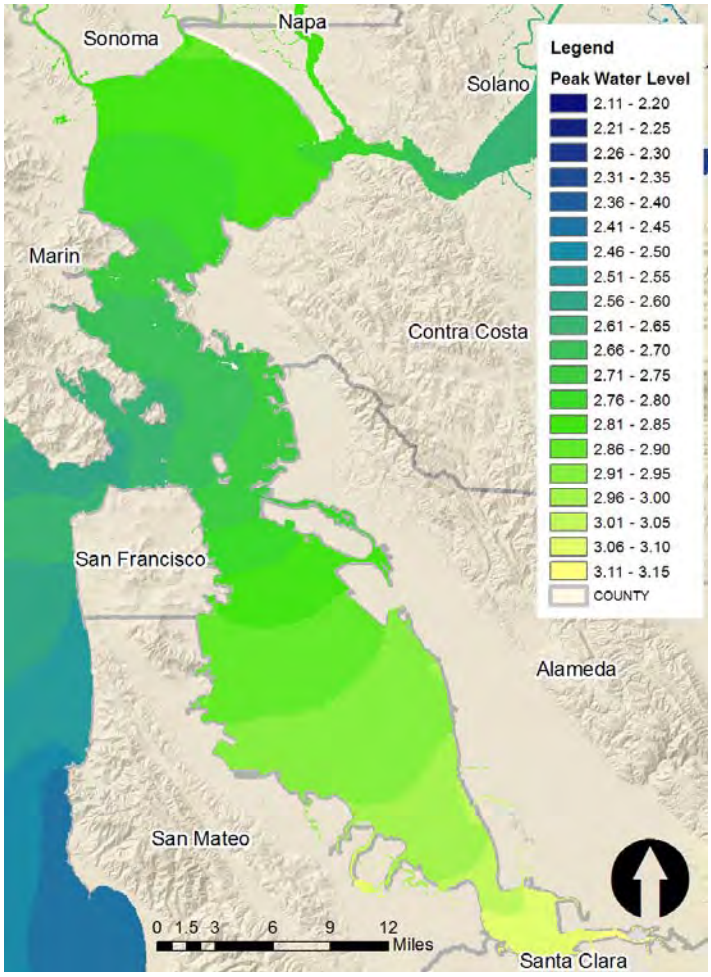

Source: Noah Knowles, USGS.

Figure 10. A 100-Year Storm Event Peak Water Surface in Raster Format. Water level elevations are in meters above the NAVD88 reference datum.

2.2 Assessing Vulnerability of the Road Network

First Responder Accessibility

Metrics can define and quantify the vulnerability of perturbed networks such as those that are inundated by flooding (Miller, 1999). Santos et al. (2010) outlines four types of reliability metrics: connectivity, travel-time, capacity, and vulnerability. Studies have successfully quantified the impact of flooding on interurban networks using county-scale data to identify critical transportation links (Sohn 2006), but the resolution and impact have remained relatively coarse. These regional-scale studies often contain modeling uncertainties that are not easily recognized, let alone quantifiable. We employ an accessibility metric at a local scale to quantify the disruption in movement in the road transportation system due to flooding. We choose accessibility to first responders to illustrate local disruption in the system, as fire stations are dispersed throughout the Bay Area in a planned attempt to evenly serve the entire population. Although we choose first responders, as their locations are planned and evenly distributed to

best serve household access in the communities, the method is universal and could serve to model the localized disruption in movement between any service and the population at large.

This metric has its roots in a class of spatial analysis models known as location- allocation models that attempt to improve or optimize *demand* conditions by altering the allocation of *supply*. These mathematical models can solve a number of conditions where demand and supply are both points (point-to-point model), where supply is mapped as a point and demand lies within a region (point-to-polygon model), or where both demand and supply are mapped as regions (polygon-to-polygon model) (Radke and Lan 2000). We apply the point to polygon model here, where supply represents first responders (fire stations) and demand are the households mapped as regions of accessibility.

The simplest location-allocation solution to the point-to-polygon model is the Voronoi or Thiessen polygon model. Here movement in the system is unconstrained and all space (demand = regions containing households) is allocated to the closest supply point (the location of the first responders). Although a powerful concept with its roots embedded in graph theory, this solution is not very realistic in a ground transportation network where movement is constrained along roads.

We employed a constrained location-allocation model and measured the accessibility of first responders (supply) to households (demand) in a region demarcated by the first responder's apparatus traveling along the shortest path, the route of least impedance or resistance, to all households in the region. We assumed that all first responders optimize the cost (defined as time travel = speed limit × distance) of travel and choose the least-cost path. In this instance, the optimum path is the shortest path that is equal to the shortest time travel path. In other words, the first responder takes the fastest route to the household.

We measured this and map a service area for all first responders. We thresholded and classified the accessibility of each first responder in increments of 1 minute for the first 10 minutes of travel. We modeled present-day conditions and generated a baseline of accessibility. We then modeled four peak water levels, as discussed previously in the sections 2.1 Potential inundation and Datums above. After each run of the model, we subtracted our baseline and calculated a surface of loss in accessibility, the impact of flood inundation on the road transportation infrastructure and local access. This metric of impact is applicable to other forms of transportation infrastructure and other service (supply) infrastructure entities, such as hospitals, schools, work, food, social services, and many other basic needs that require movement from an origin to a destination along a transportation network.

Node-To-Node Accessibility Impacts on the Major Traffic Corridors

The impact of inundation due to rising sea levels and extreme storm events will be felt far beyond the local neighborhoods that are flooded. The Bay Area's transportation network includes and is critically dependent on several major highways that serve as not only the main building blocks of its topological skeleton, but also the main regional corridors of traffic flow. As a result, potential inundation of some of these major road sections has the potential of disrupting traffic flow across the entire region.

Traversing a region involves an origin-destination event that would likely begin in a local neighborhood network, travel the shortest-time path to the nearest intersection (on ramp node) of the major highway system, travel the shortest-time path along that regional system to the nearest intersection (off ramp node) of the local destination network, and proceed along the shortest-time path route to the final destination. Impacts due to inundation on the major highway corridors would serve to disrupt regional travel flows. We modeled this potential impact on regional traffic flow by measuring the disruption of the major node-to-node travel times through various inundation scenarios. Figure 11 represents the major nodes and links of the major traffic corridors in the region that are at risk of potential inundation due to rising sea levels and serves as our map base in this regional analysis. Although we measured the travel time impact from node-to-node in this major highway network, we included the entire local and regional network in our shortest-time path calculations.

Applying the point-to-point location-allocation model, we mapped each supply node as a major intersection in our regional network sample (mapped in Figure 11) and demand as all the other major nodes in the regional network. We chose the nine counties surrounding the San Francisco Bay as the extent of our transportation network region. We calculated the point-to-point accessibility time for all node pairs using the current posted traffic speeds. Although all traffic condition scenarios throughout the day, week, month, and year could be modeled using our method, it would only serve to sensitize a variety of road condition scenarios unrelated to inundation and not relevant to the current study objectives. We modeled through a series of inundation scenarios and report the node-to-node impact on accessibility between the major corridor intersections.

We quantified regional vulnerability by calculating the loss of accessibility between nodes (highway intersections). We calculated the travel time (in minutes) in normal condition and the travel time under the potential inundation. In order to depict the loss of accessibility, we used the travel time increment under different conditions as shown below.

$$Increment\ of\ travel\ time = \frac{Travel\ time\ under\ inundation}{Travel\ time\ in\ normal\ condition}$$

By using this metric, we assessed the vulnerability of road network connectivity around the Bay Area, which is exposed to the inundation due to sea-level rise and extreme storm events. Because we mainly focused on physical connectivity and the increment of travel cost (time or distance), we did not include any travel forecast (or behavior) model in our approach.

The failure of a specific road link causes more severe consequences when the alternative route requires more travel time. In addition, when a greater demand exists, the importance of the link increases. Hence, we calculated the weighted loss of accessibility by including traffic volume information (annual average daily traffic: AADT) in our approach, as shown below:

$$Weighted\ increment\ of\ travel\ distance = increment\ of\ travel\ distance \times AADT$$

We estimated the increment of travel distance for a specific link by subtracting the travel distance (in meters) under the normal condition from the travel distance under the disruption (inundation). Then we multiplied by the AADT value for the link to estimate the weighted loss of accessibility. We used traffic volume data (2010) from Caltrans (http://traffic-counts.dot.ca.gov/) to extract AADT for our analysis. Because our approach calculated node-to-node accessibility, multiple AADT values might exist for a specific link. As we assume complete loss of the connectivity between two nodes for our calculation, we used the maximum AADT value among the AADT values of the route segments.

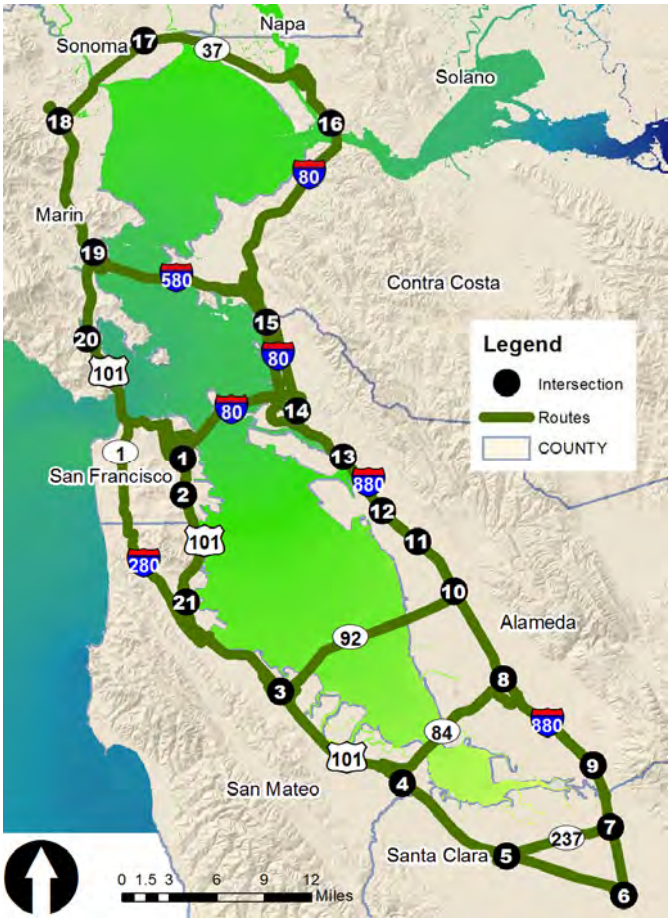

Figure 11. The Nodes and Links of the Major Traffic Corridors in the Region of Potential Inundation Due to Rising Sea Levels.

Hinterland Accessibility

Finally we employed a similar point-to-polygon location-allocation model to the one described in the section 2.2 First responder accessibility to measure the impact of accessibility in the hinterland of the major system. This models the local neighborhood network from origin to the nearest (in time) major highway node (on ramp), and it models the local neighborhood network from the major highway nodes (off ramps) to the final destination. Here the major highway intersections are the supply points and the regional hinterland the demand.

Section 3: Results

3.1 Potential Inundation of Transportation Infrastructure

Roads and Rails

By using ground elevation models, digital surface models, and GIS data layers, we estimate the length of roads affected by inundation. The high water levels of a 100-year extreme event are projected with sea-level rise levels of 0 m, 0.5 m, 1.0 m, and 1.4 m. Under current conditions (see Table 5), we estimate 594.5 miles (49.3 miles of highways and 545.2 miles of local streets) of roads are at risk of a 100-year extreme storm event $PLW_{(0)}$. With $PWL_{(1.4)}$, that is a 1.4 m sea-level rise and 100-year extreme storm event, 1,688.2 miles of roads (169.5 miles of highways and 1,518.7 miles of local streets) are at risk. With $PWL_{(1.4)}$, the length of roads at inundation risk increases nearly three times compared to $PWL_{(0)}$, the 100-year flooding event without sea-level rise.

In this study, we estimate the length of roads by using not only elevation (depth) data, but also water path (connectivity to the water of the San Francisco Bay). Table 5 shows the results of the road inundation estimation which incorporates both the depth data and water path. In contrast, Table 6 shows the results of the road inundation estimation by using depth-only data (without water path). As expected, when we applied the depth-only method (see Table 6), all the results are overestimated regardless of water levels. However, the difference of the inundation length estimation between these two methods decreases as the water level increases. As the water level goes up, blocked water paths (by flood protection structures) can be connected, if the water level is higher than the structure. Hence, when the water level is low, more areas are determined as non-inundation because these areas are not connected to the San Francisco Bay or Pacific Ocean. When we use the depth-only method, the estimated length of risk is 744.2 miles and this approach overestimated by 25 percent (149.7 miles) compared to the extreme storm event (with no sea-level rise). Figure 12 shows the miles of highways and local roads in the Bay Area that are vulnerable to a100-year extreme event.

Table 5. Miles of Road at Risk to a 100-Year Extreme Event by County and Type (Highway and Local) Using Water Depth and Water Paths Analysis

	Current risk		Risk with sea-level rise					
			0.5 m		1.0 m		1.4 m	
COUNTY	Highways (miles)	Roads (miles)	Highways (miles)	Roads (miles)	Highways (miles)	Roads (miles)	Highways (miles)	Roads (miles)
ALAMEDA	1.0	46.4	12.4	195.3	21.6	358.5	31.7	471.3
CONTRA COSTA	0.1	3.5	0.1	11.3	2.7	29.1	4.2	49.4
MARIN	14.1	92.6	19.7	142.5	25.0	185.8	28.4	210.8
NAPA	0.9	5.2	1.0	7.6	1.0	9.6	1.2	14.4
SAN FRANCISCO	0.2	2.9	0.6	11.0	3.1	40.1	4.3	52.3
SAN MATEO	15.2	256.9	36.0	341.6	57.3	384.4	61.0	407.6
SANTA CLARA	5.9	75.5	8.7	113.6	9.9	142.6	11.0	177.6
SOLANO	4.2	7.0	6.7	19.3	14.6	48.7	15.9	59.2
SONOMA	7.6	55.2	8.5	65.3	10.1	72.1	11.9	76.2
Total	49.3	545.2	93.7	907.5	145.4	1270.8	169.5	1518.7

Table 6. Miles of Road at Risk to a 100-Year Extreme Event by County and Type (Highway and Local) Using Water-Depth Only

	Current risk		Risk with sea-level rise					
			0.5 m		1.0 m		1.4 m	
COUNTY	Highways (miles)	Roads (miles)	Highways (miles)	Roads (miles)	Highways (miles)	Roads (miles)	Highways (miles)	Roads (miles)
ALAMEDA	3.0	101.5	13.3	231.7	22.9	396.0	33.4	496.2
CONTRA COSTA	2.2	6.7	2.4	18.1	2.9	37.3	4.3	54.7
MARIN	14.5	108.8	19.9	153.7	25.0	191.7	28.4	213.5
NAPA	0.9	5.9	1.0	7.7	1.0	10.3	1.2	16.0
SAN FRANCISCO	0.3	6.8	1.1	20.6	3.1	51.1	4.3	64.1
SAN MATEO	16.4	287.6	37.2	349.5	57.5	389.8	61.2	412.2
SANTA CLARA	7.0	98.3	8.9	134.4	10.1	178.6	11.2	206.2
SOLANO	5.3	14.6	10.4	31.5	14.9	50.0	16.3	60.4
SONOMA	7.6	57.0	8.5	66.3	10.2	72.6	12.1	77.5
Total	57.1	687.1	102.7	1013.5	147.7	1377.3	172.5	1600.7

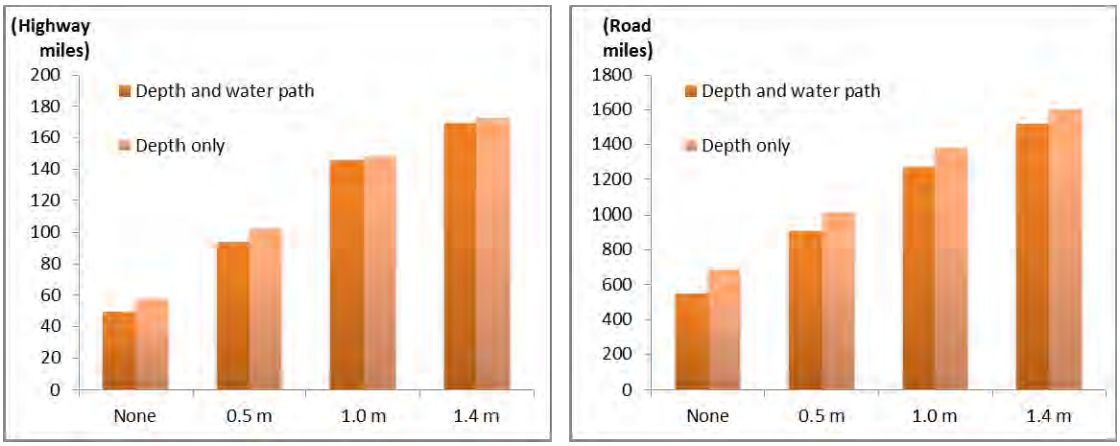

(a) (b)

Figure 12. Miles Vulnerable to a 100-Year Extreme Event in the San Francisco Bay Area. (a) Highways, (b) local roads.

The rail system in the Bay Area is important because the rail system transports a large amount of freight and people. Hence, disruption of operations brings significant impact and consequence to the region. We estimated the length of rails at risk to a 100-year flood event combined with different sea-level rise scenarios. With $PWL_{(1.4)}$, 155.7 miles of railways will be potentially at risk. With no SLR and a 100-year flood ($PWL_{(0)}$), 36.3 miles of railways will be at risk (see Table 7). Table 7 shows the amount of rails at risk when we use both water depth and water path analysis; whereas, Table 7 only uses water depth in determining inundation areas.

Table 8 shows the results from using the depth-only method, which overestimates the amount of rails at risk.

Table 7. Miles of Rails at Risk to a 100-year Extreme Storm Event by County Using Water Depth and Water Paths Analysis

COUNTY	Current risk	Risk with sea-level rise		
		0.5 m	1.0 m	1.4 m
ALAMEDA	6.9	23.4	46.7	62.7
CONTRA COSTA	0.2	4.5	10.1	18.9
MARIN	9.0	14.5	18.7	19.7
NAPA	3.2	6.5	7.4	8.4
SAN FRANCISCO	0.0	1.2	1.9	2.2
SAN MATEO	4.9	8.7	10.7	12.7
SANTA CLARA	4.6	5.6	6.9	7.4
SOLANO	1.1	1.8	4.4	5.0
SONOMA	6.4	12.2	17.3	18.8
Total	36.3	78.4	124.0	155.7

Table 8. Miles of Rails at Risk to a 100-Year Extreme Storm Event by County Using Water Depth-Only Data

COUNTY	Current risk	Risk with sea-level rise		
		0.5 m	1.0 m	1.4 m
ALAMEDA	11.0	26.8	48.6	63.1
CONTRA COSTA	1.0	5.3	10.9	19.3
MARIN	10.2	15.0	18.7	19.8
NAPA	4.4	6.6	7.7	8.4
SAN FRANCISCO	0.6	1.3	1.9	2.2
SAN MATEO	5.8	9.9	12.9	15.6
SANTA CLARA	5.9	7.4	8.9	9.6
SOLANO	2.1	3.3	5.3	6.1
SONOMA	6.4	12.2	17.4	18.8
Total	47.5	87.8	132.3	163.0

Ports and Airports

It is evident that sea-level rise and flooding pose risks to the Bay Area's ports and airports, primarily because they are in low lying coastal areas. Even if these facilities are adequately protected by levees, dykes, roads, or other human-made barriers (as seen in Figure 9), for current climate conditions, there is increased risk of failure and overtopping as a result of projected SLR in combination with 100-year flooding.

Figure 13 gives a synoptic view of the areas in the San Francisco Bay region we project to be impacted by a 100- year storm event in combination with either no sea-level rise ($PWL_{(0)}$) or 1.4m sea-level rise ($PWL_{(1.4)}$). It is clear that the ports and airports of the San Francisco Bay region are impacted under one or both of these scenarios. This is discussed in more detail below. There is generally good correspondence between Figure 13 here and Figure 5a in Knowles (2009, 2010). Our figure shows a larger extent of area affected by inundation under $PWL_{(1.4)}$ in the North Bay, particularly in Marin and Sonoma counties. Knowles (2009, 2010) excluded wetlands from his analysis, whereas we did not. Thus our work depicts the wetlands of the south Bay as inundated in a 100-year extreme storm. The differences between our work and Knowles' at the Oakland International Airport and San Francisco International Airport are discussed below.

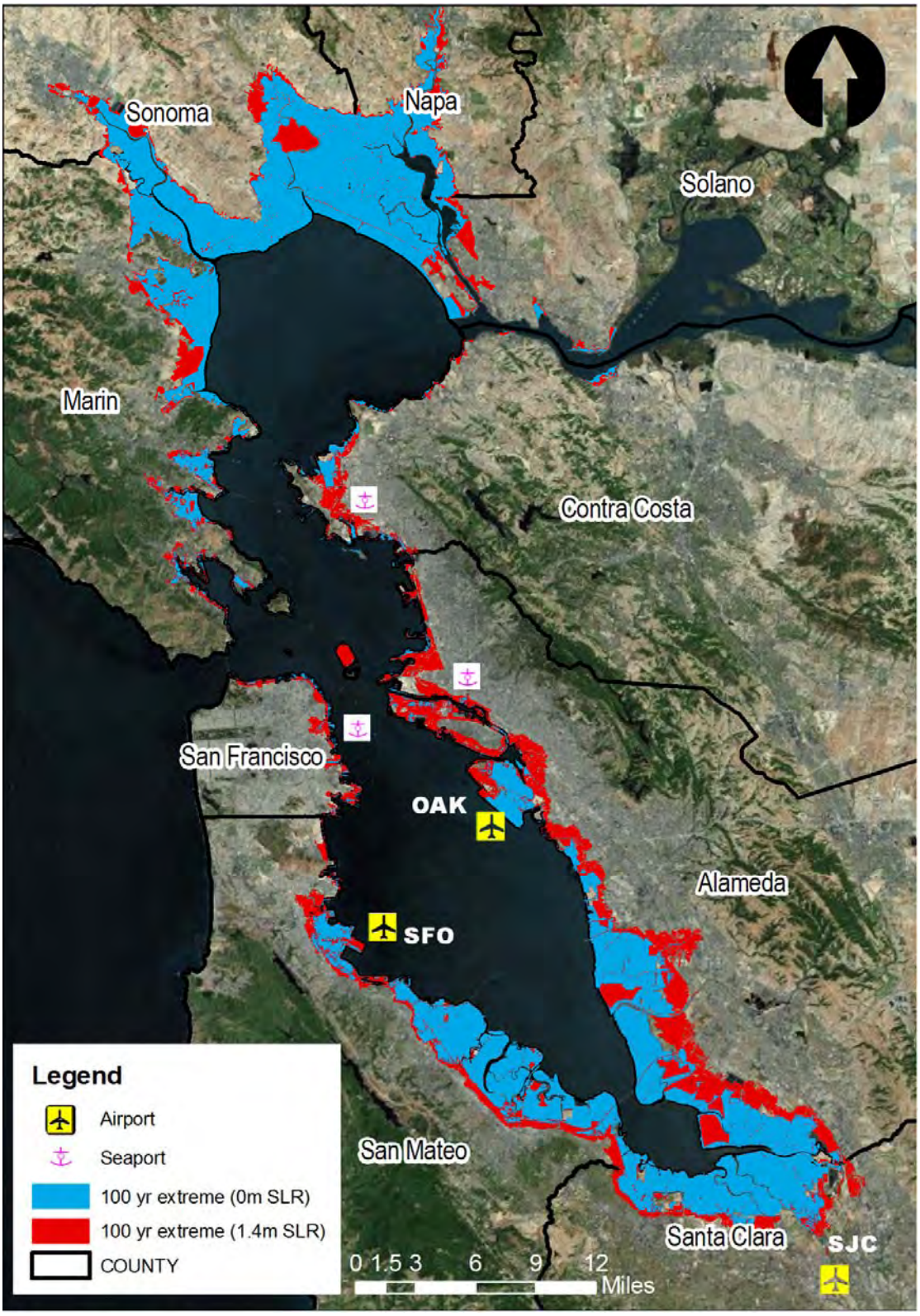

Figure 13. Locations in the San Francisco Bay Area Projected to be Impacted by a 100-Year Extreme Storm Event without and with 1.4 m Sea-Level Rise.

Our DEM shows that large portions of the runways at the SFO (see Figure 14) and the OAK (not depicted) are less than 2.6m above the NAVD88 reference datum. Predicted water levels for the 100-year extreme storm event ($PLW_{(0)}$) are approximately 2.8–3.0 m above the NAVD88 datum throughout much of the Bay (see Figure 10). Thus extreme storm events alone may be sufficient to cause inundation at these airports.

Figure 14 shows no inundation at the (SF0) when the water level reaches 2.4 m above the reference datum (NAVD88). Although a large portion of the airport is lower than 2.4 m above the reference datum, there is no inundation inside of the airport property at this water height because there is a partial seawall (BCDC 2009). Figure 15 shows the potential for inundation when the water height reaches 2.5 m near SFO. The DEM for the airport shows the north part of SFO is particularly vulnerable because the boundaries of the north part of the airport are lower than other areas, as revealed by the DSM of the area (In Figure 15, the white arrows show the initial inundation water paths).

We calculated the ratio of runways at risk to a 100-year extreme storm event under various SLR values. Although there are several critical structures and facilities in airports, we calculated the inundation for the runways because this is a good representation of airport functions. Particular attention should be paid to the fact that the runways of both SFO and OAK are at risk for a 100-year flood event even without any sea-level rise (Figure 16).

All runways will be nearly 100 percent inundated with $PWL_{(1.0)}$ and entirely inundated with $PLW_{(1.4)}$. For the Oakland International Airport, the runways at the North Field are more vulnerable because these runways are located on the lower elevations (see BCDC 2011 for inundation depth at OAK with a 0.4 m SLR in conjunction with 100-year flood event). However, all runways at OAK will be inundated by a 100-year storm event without any sea-level rise ($PWL_{(0)}$). Of course it is likely that the airports will take actions to mitigate or reduce these potential effects.

In addition to sea-level rise that exceeds 1m, there are other pathways, not fully explored in this paper that could cause flooding. For example, high tides in the Bay routinely exceed 2 m above NAVD88, as evidenced by MHHW statistics compiled by NOAA (Figure 7). When large storms occur, they can add an additional component of anomalous sea level from barometric and wind-driven effects. This anomalous component, under extreme conditions, can add 0.5 m or more to astronomical tide levels. Thus, if mean sea level rises 0.5 m, and a large storm producing 0.5 m of anomalous sea level coincides with 2 m astronomical tides, the water level will reach 3 m, which is sufficient to cause inundation at SFO and OAK. This calculation ignores the effect of wind waves, which would add to the excess water levels and make such an event even more extreme.

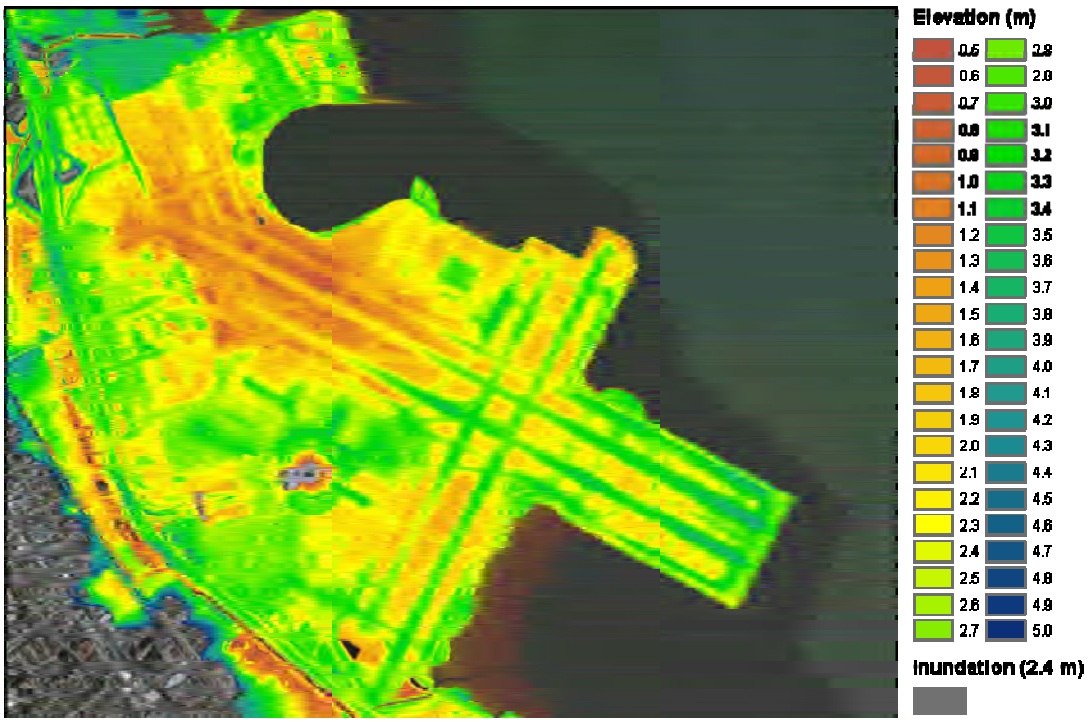

Figure 14. San Francisco International Airport. The potential inundation with the peak water level 2.4 m above the NAVD88 reference datum.

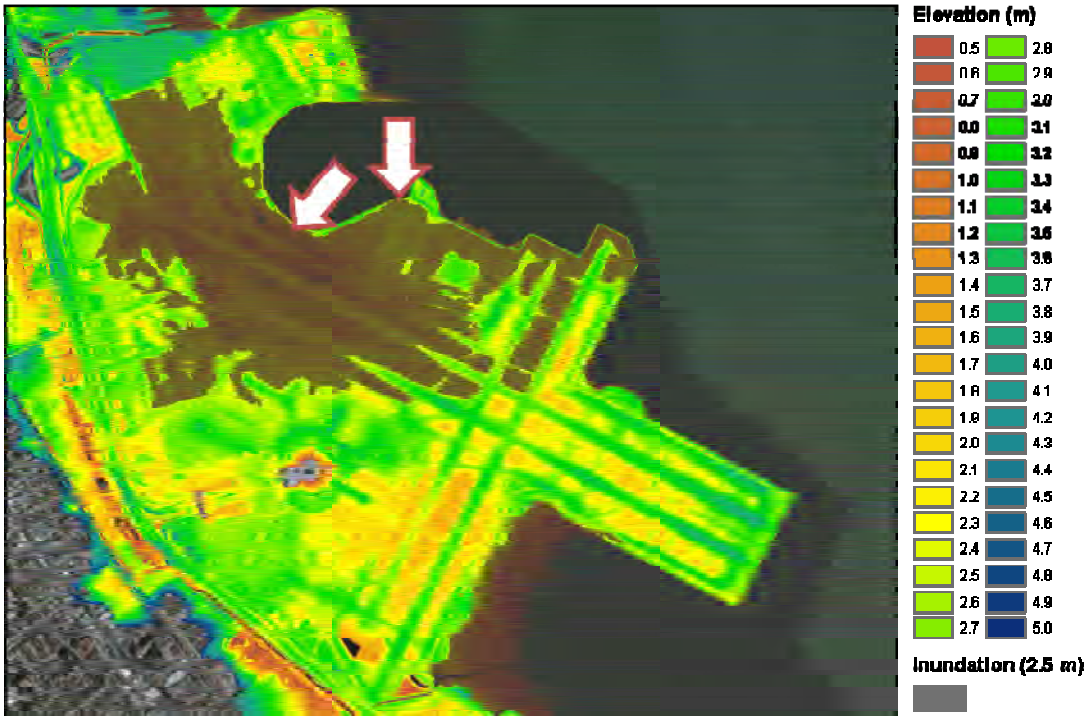

Figure 15. San Francisco International Airport. The potential inundation with the peak water level 2.5 m above the NAVD88 reference datum.

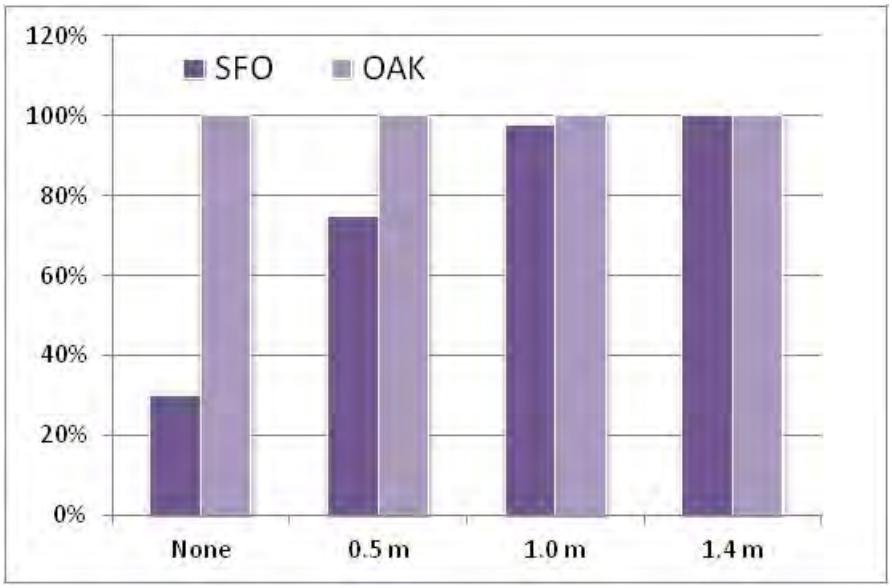

Figure 16. The Ratio of SFO and OAK Runway at Risk to a 100-Year Flood Event under Different Sea-Level Rise Values (none or 0 m, 0.5 m, 1.0 m, and 1.4 m).

The Port of Oakland

A difference between our findings (Figure 17) and prior estimates from Knowles (2009, 2010) (Figure 18) is worth mentioning. In the loop area near the Port of Oakland (7th Street and Maritime Streets; see Figure 19 for street names) slightly to the left of the center of the figure, Knowles predicts some areas of inundation (in red) with $PWL_{(1.5)}$ (Figure 18). In the current study (Figure 17), even at the highest peak water level examined ($PWL_{(1.4)}$) there is no inundation in this loop area. The approach to the Bay Bridge is at the north end of the Oakland Outer Harbor. Knowles predicts some inundation on both sides of the Bay Bridge approach with $PWL_{(0)}$ (see Figure 18). Our analysis indicates less flooding in this area at $PWL_{(0)}$ and more flooding for $PWL_{(0.5)}$ compared to Knowles. The area below the northern boundary of 7th Street experiences more extensive flooding at $PWL_{(1.0)}$ in Knowles' work than in ours with $PLW_{(1.0)}$. The same can be observed using $PWL_{(1.5)}$ and $PWL_{(1.4)}$, respectively. These same observations hold in the area directly north of 7th Street and bounded by the Nimitz freeway. Clearly the patterns are broadly similar, but the distributions of affected areas are different between these two studies. When results differ, it generally takes higher water levels to achieve inundation in our analysis than indicated in Knowles findings. We posit that this is due to the differences in the resolution of the DEMs used in these two studies and our use of the DEM, DSM, and water path (not solely water depth) in determining inundation areas.

Figure 17. The Port of Oakland. This delineates the area at risk of a 100-year flood event under different sea-level rise elevations (none or 0 m, 0.5 m, 1.0 m, and 1.4 m) in the current study.

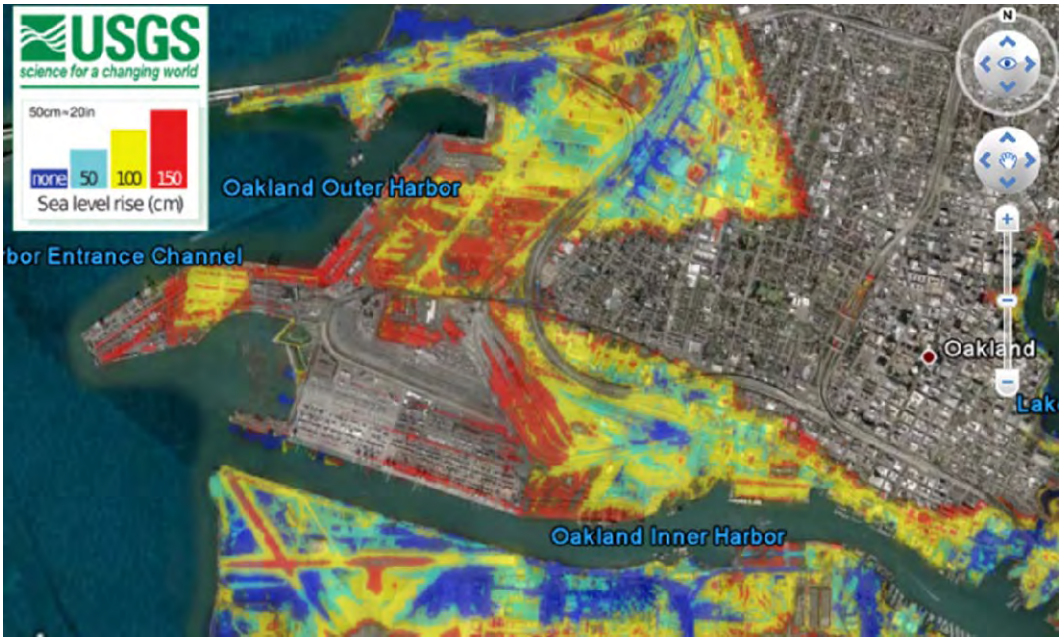

Source: USGS CASCaDE Project

Figure 18. Areas of Inundation at the Port of Oakland, Taken from the USGS CASCaDE Project (http://cascade.wr.usgs.gov/data/Task2b-SFBay/index.shtm) That Has Publicly Available Data Generated by Knowles (2009–2010). This delineates the area at risk of a 100-year flood event under different sea-level rise elevations (none or 0 m, 0.5 m, 1.0 m, and 1.5 m).

Source: Google Earth

Figure 19. Roads of the Port of Oakland.

In Figure 20, we show the proportion of the Bay Area's three major ports that are inundated by our scenarios. With a 100-year flood with no sea-level rise ($PWL_{(0)}$), the Port of Oakland has virtually no portion flooded; about 10 percent of the Port of Richmond is flooded, and more than 25 percent of the Port of San Francisco is flooded. With $PWL_{(1.4)}$ the flooded area exceeds 50 percent at Oakland, is slightly less than 50 percent at Richmond and about 80 percent at San Francisco. Clearly these percent areas inundated with 100-year flooding are substantial by the time we reach 0.5 m of sea-level rise.

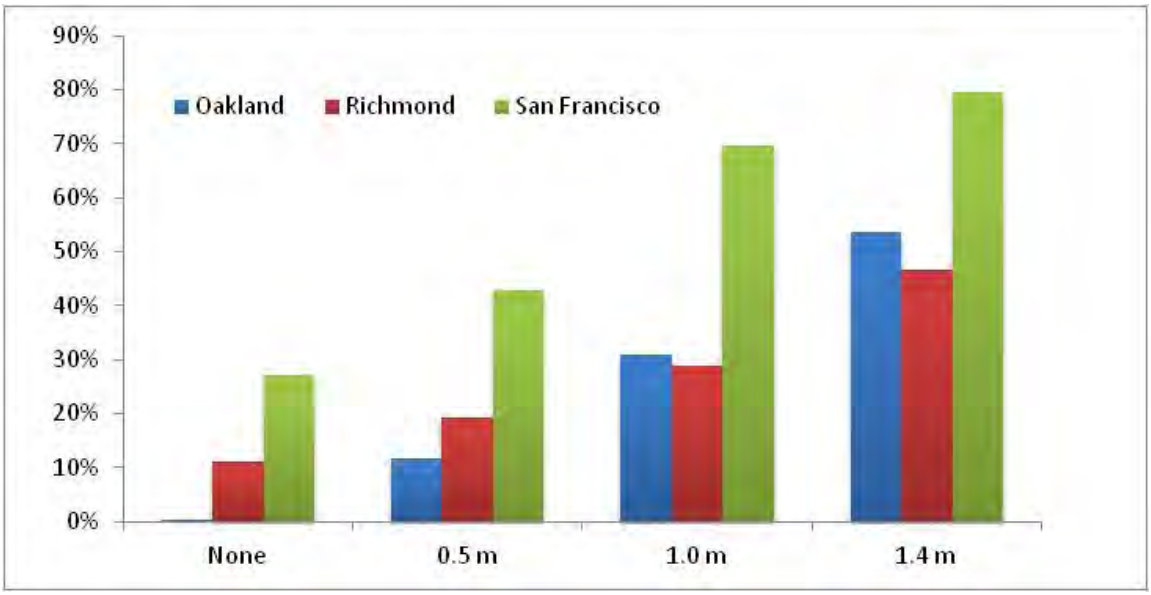

Figure 20. The Ratio of Areas of the Ports of Oakland, Richmond, and San Francisco at Risk to a 100-Year Flood Event under Different Sea-Level Rise (none or 0 m, 0.5 m, 1.0 m, and 1.4 m).

3.2 Loss of Accessibility by Inundation

As a quantitative measure of the vulnerability of the road network under potential inundation, we calculated the loss of accessibility by disruption. Below we report on the results of our accessibility analysis in two areas, Richmond in Contra Costa County and northern Santa Clara, by zooming in and mapping the detail of the analysis. We then zoom out and report and graph the overall results for the entire greater Bay Area.

Our approach for calculating the accessibility metric focuses on local accessibility when the density of the service providers (in this study, fire stations) is quite good and the locations of service providers are spatially well distributed over the service area, making the providers appear to be ubiquitous to the population around the Bay Area. There is great loss and devastation to homes and fire stations themselves due to different levels of flooding events. However, while some local networks experience accessibility impacts, there is no dramatic or unexpected major loss of accessibility under potential inundation in the Bay region as a whole. In our analysis for this area, there is no region that is expected to have excessive accessibility loss due to different levels of flooding events. It appears that as fire stations (supply) are inundated, so are properties (demand), and there is relatively little disruption in local access in the non-inundated areas. Of course, in the immediate aftermath of inundation there are local effects that are real and burdensome. When we talk about there being little disruption in local access, we are really speaking about equilibrium results after the hardship of the short-term effects diminishes.

With a 100-year storm event with no SLR ($PWL_{(0)}$), the greater Bay region will lose access to 16 first responder fire stations (Table 9). That figure jumps to 36 with $PWL_{(1.4)}$. In both of these

scenarios, Marin and Napa county account for over 60 and 50 percent, respectively, of the first responder fires stations losses to these events. In the most extreme case, Alameda County loses 7 fire stations accounting for approximately 20 percent of the losses. The area (km^2) experiencing a 1–9 minute time delay grows by a factor of 2.5x from $PWL_{(0)}$ to $PWL_{(1.4)}$ (Table 10). The area that is non-accessible grows from approximately 10 km^2 with $PWL_{(0)}$ to nearly 300 km^2 with $PWL_{(1.4)}$.

Table 9. Loss of First Responder Fire Stations in the San Francisco Bay Study Region as a Function of Peak Water Levels

COUNTY	Peak Water Level			
	0.0 m	0.5 m	1.0 m	1.4 m
ALAMEDA	2	3	5	7
MARIN	4	6	8	9
NAPA	1	1	1	1
SAN FRANCISCO	1	1	3	4
SAN MATEO	6	9	9	10
SANTA CLARA	2	3	3	3
SOLANO	0	0	1	1
SONOMA	0	0	1	1
Total	16	23	31	36

Table 10. Area (km^2) in Accessibility Classes in the San Francisco Bay Study Region. Time delay is for additional minutes above the current (normal) commute conditions due to delays caused by peak water levels.

Time delay	Peak Water Level			
to access	0.0m	0.5m	1.0m	1.4m
1 minute	46.07	58.08	78.41	82.33
2 minute	16.10	25.26	33.40	39.49
3 minute	7.98	13.75	21.98	27.00
4 minute	4.50	9.85	19.01	19.46
5 minute	2.92	6.90	12.05	17.30
6 minute	2.29	4.47	7.37	10.23
7 minute	1.85	3.36	4.68	6.25
8 minute	0.72	1.71	2.55	2.99
9 minute	0.16	0.56	0.69	0.82
Subtotal 1-9 min.	82.59	123.94	180.14	205.87
Non-Accessible	9.83	91.90	258.06	291.41

Loss of Accessibility in Richmond, California

Figures 21(a) to 21(e) represent the accessibility metric of fire stations under a 100-year extreme storm event and different sea-level rise scenarios: none or 0 m, 0.5 m, 1.0 m, and 1.4 m, respectively. In these figures, the gradual color change represents the different levels of accessibility. The green color represents good accessibility (travel time in minutes) and the red color represents poor accessibility. Figure 21(a) represents the accessibility measure under the normal condition (without any disruption). We use this accessibility metric as a baseline to calculate the change of the accessibility under different flooding and sea-level rise conditions.

With a 100-year extreme storm event plus 0.5 meter sea-level rise ($PWL_{(0.5)}$) we see the beginning of road flooding in the western most section of Richmond (Figure 21(c)). Richmond Lane and North Castro Street become impassable blocking road access to this area. With 1.0 meter or more sea-level rise and a 100-year extreme storm event ($PWL_{(1.0)}$), access from Point Richmond to Richmond proper becomes inaccessible. The majority of inland areas do not become inundated because they are naturally located away from the shoreline.

Figure 21(f) shows the change in accessibility by a 100-year extreme storm event and sea-level rise with a 1.4 m water level ($PWL_{(1.4)}$) relative to normal conditions. The yellow color means no change and the gradual color change toward red represents the additional amount of access time compared to the access time under the normal condition (without any sea-level rise or flooding). As we expect, the inland area does not show any change (colored in yellow).

The major effect from a $PWL_{(1.4)}$ event is the large increment of non-accessible service area which is displayed in black. In addition, the areas to the southeast of Point Richmond show large increments in access time (4 minutes or more) from the sole fire station in Point Richmond. This occurs because this large flooding event blocks Cutting Boulevard. Because Cutting Boulevard is flooded, the southeastern route from the fire station (located in the north central part of Point Richmond) to the southern part of Point Richmond is not fully accessible. If these roads are blocked, the only access from the fire station to the southern part of Point Richmond is the road located on the western shoreline, so that fire fighters need to select a less efficient route under the flooding event.

(a)


Tara Hills
El Sobrante
San Pablo
North Richmond
East Richmond Heights
Richmond
El Cerrito
580
80
Legend
Fire Stations
Water (no SLR)
Streets
SPEED
1; 5
20; 25
35
45
55
Accessibility
minute
1
2
3
4
5
6
7
8
9
10
0 0.5 1
Miles

(b)


Tara Hills
El Sobrante
San Pablo
North Richmond
North Castro Street
East Richmond Heights
Richmond Lane
Richmond
El Cerrito
580
80
Legend
Fire Stations
Water (0.5m SLR)
Streets
SPEED
1; 5
20; 25
35
45
55
Accessibility
minute
1
2
3
4
5
6
7
8
9
10
0 0.5 1
Miles

(c)

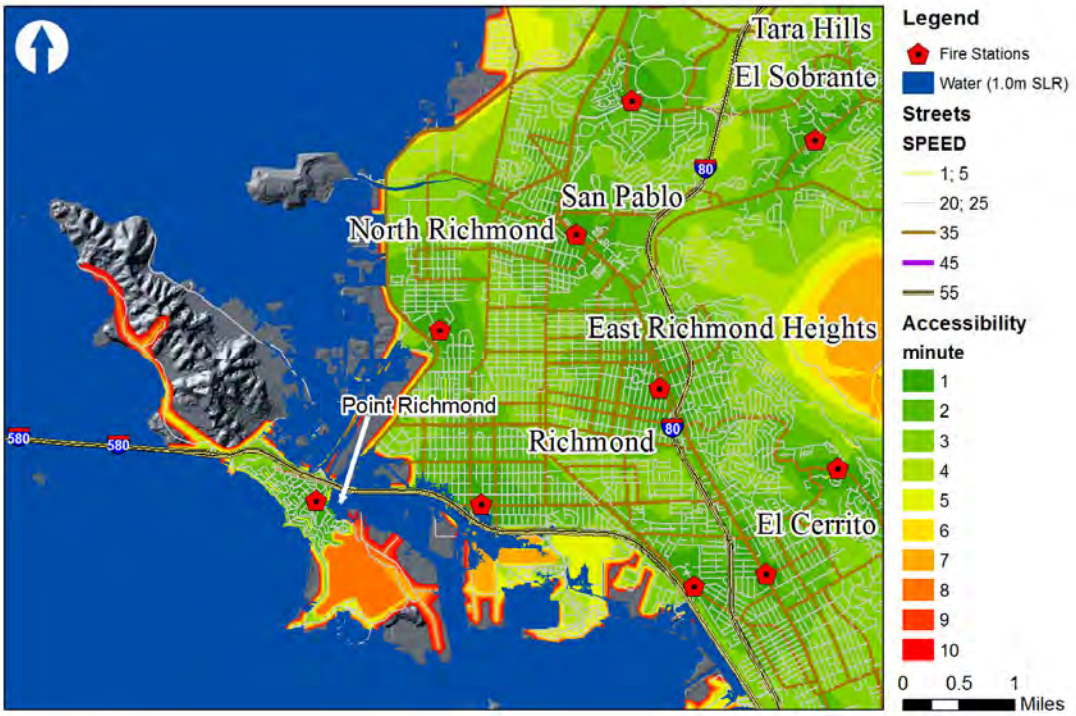
Tara Hills
El Sobrante
San Pablo
North Richmond
East Richmond Heights
Point Richmond
Richmond
El Cerrito
580
80
Legend
Fire Stations
Water (1.0m SLR)
Streets
SPEED
1; 5
20; 25
35
45
55
Accessibility
minute
1
2
3
4
5
6
7
8
9
10
0 0.5 1
Miles

(d)

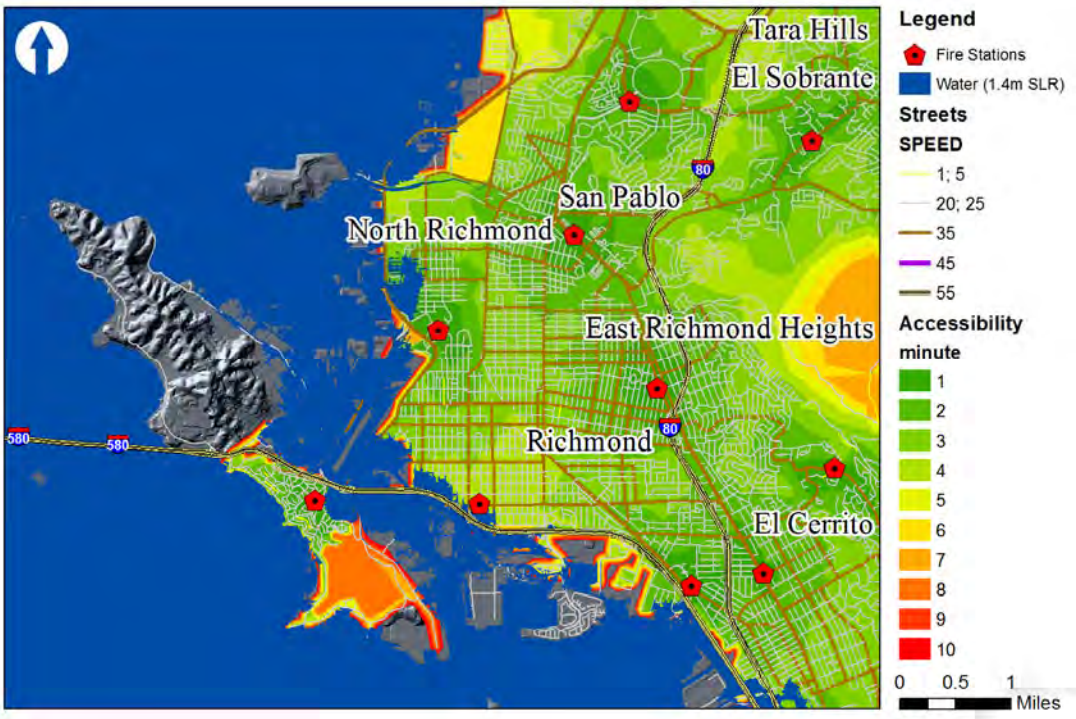
Tara Hills
El Sobrante
San Pablo
North Richmond
East Richmond Heights
Richmond
El Cerrito
580
80
Legend
Fire Stations
Water (1.4m SLR)
Streets
SPEED
1; 5
20; 25
35
45
55
Accessibility
minute
1
2
3
4
5
6
7
8
9
10
0 0.5 1
Miles

(e)

(f)

Figure 21. Richmond First Responder Accessibility in Minutes. (a) Under normal conditions, (b) under a 100-year extreme storm event with no sea-level rise, (c) under a 100-year extreme storm event with 0.5 meter sea-level rise, (d) under a 100-year extreme storm event with 1.0 meter sea-level rise), (e) under a 100-year extreme storm event with 1.4 meter sea-level rise, and (f) the change in accessibility under a 100-year extreme storm event with 1.4 m sea-level rise relative to normal conditions.

Loss of Accessibility in Santa Clara, California

For the Santa Clara area, we calculate the same accessibility metric and acquire similar results. Figures 22(a)-22(e) show the accessibility of fire fighters in the northern part of Santa Clara County. In these figures, the gradual color change represents the different levels of accessibility. The green color represents good accessibility (time in minutes) and the red color represents poor accessibility. Figure 22(a) represents the accessibility measure under the normal condition (without any disruption). Figure 22(b), Figure 22(c), Figure 22(d) and Figure 22(e) represent different accessibility measures under a 100-year extreme storm event and different sea-level rise scenarios – none or 0 m, 0.5 m, 1.0 m, and 1.4 m, respectively.

The results of our analysis show that one fire station is lost with a 100-year extreme storm event with no sea-level rise ($PWL_{(0)}$). With 0.5 m sea-level rise and a 100-year extreme storm event ($PWL_{(0.5)}$), an additional fire station is inundated. However, the loss of service at these stations does not directly impact the calculation of the robustness of the road network accessibility, as the distribution of fire stations (supply) in this region is evenly dispersed with respect to the demand.

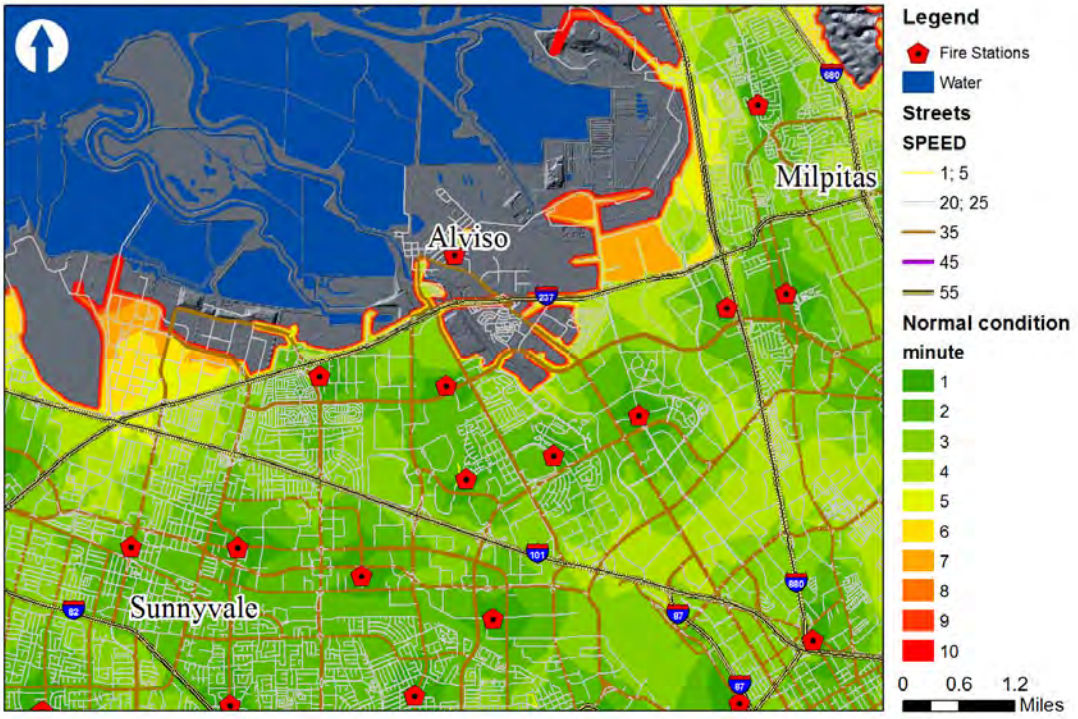
Legend
Fire Stations
Water
Streets
SPEED
1; 5
20; 25
35
45
55
Normal condition
minute
1
2
3
4
5
6
7
8
9
10
0 0.6 1.2
Miles
Milpitas
Alviso
Sunnyvale

(a)

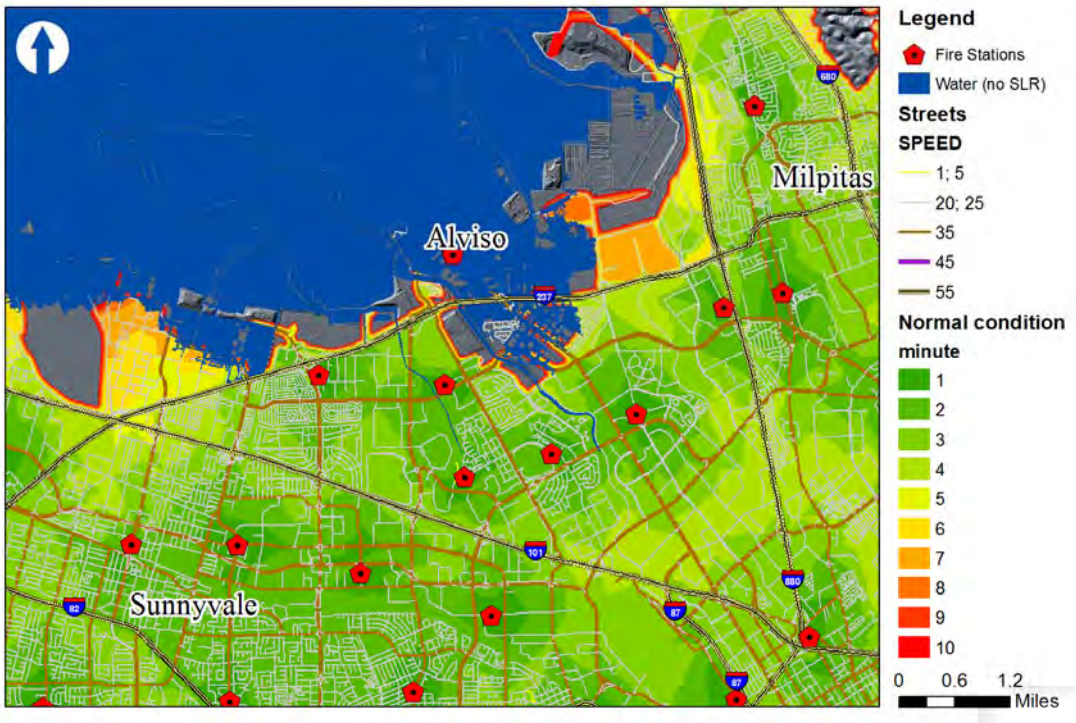
Legend
Fire Stations
Water (no SLR)
Streets
SPEED
1; 5
20; 25
35
45
55
Normal condition
minute
1
2
3
4
5
6
7
8
9
10
0 0.6 1.2
Miles
Milpitas
Alviso
Sunnyvale

(b)


Legend
Fire Stations
Water (0.5m SLR)
Streets
SPEED
1; 5
20; 25
35
45
55
Accessibility
minute
1
2
3
4
5
6
7
8
9
10
0 0.6 1.2
Miles
Milpitas
Alviso
Sunnyvale

(c)

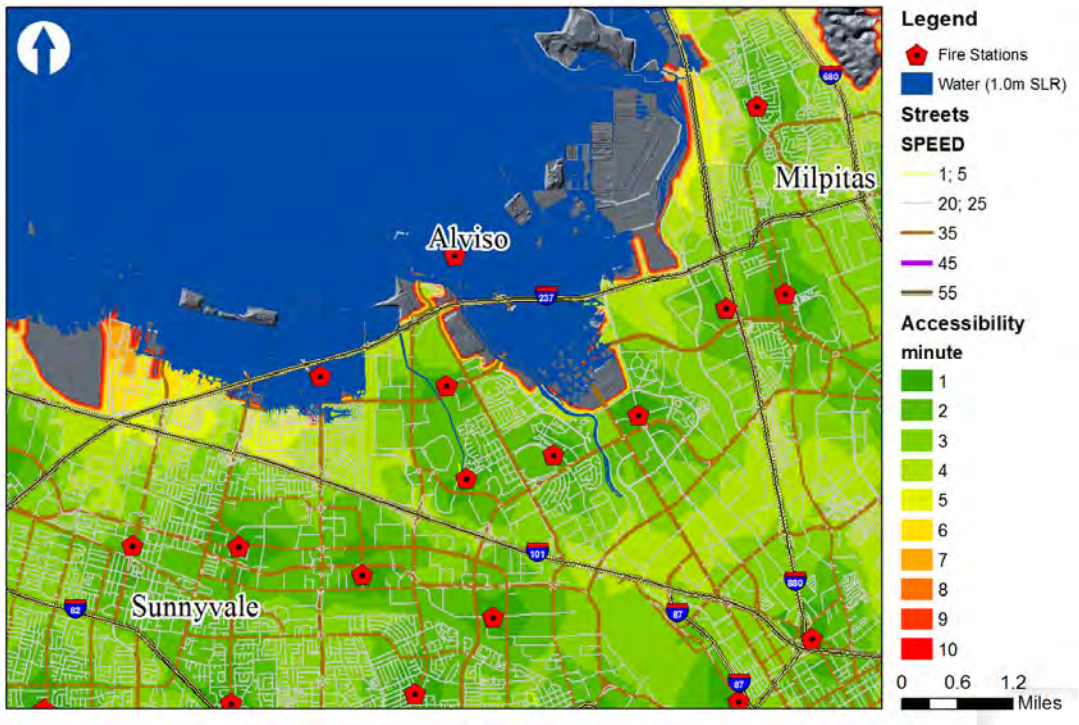
Legend
Fire Stations
Water (1.0m SLR)
Streets
SPEED
1; 5
20; 25
35
45
55
Accessibility
minute
1
2
3
4
5
6
7
8
9
10
0 0.6 1.2
Miles
Milpitas
Alviso
Sunnyvale

(d)

(e)

Figure 22. Santa Clara First Responder Accessibility. (a) Under a normal conditions, (b) under a 100-year extreme storm event with no sea-level rise, (c) under a 100-year extreme storm event with a 0.5 m sea-level rise, (d) under a 100-year extreme storm event with a 1.0 m sea-level rise, and (e) under a 100-year extreme storm event with a 1.4 m sea-level rise.

We conducted our local accessibility analysis for the entire San Francisco Bay Region and reported our results. Figure 23 below shows the reduction in accessibility in minutes under a 100-year storm event with 1.4 m sea-level rise ($PWL_{(1.4)}$) for the greater Bay region. Under this scenario, first responder fire stations become inaccessible in all counties except Contra Costa. The greatest concentration of losses occurs in Marin, San Mateo, and Alameda Counties. As discussed previously, the loss of service at many of these stations does not translate into reductions in accessibility at neighboring stations. That is, as the supply of fire stations is being reduced, so too is the demand from homeowners who are now isolated or removed due to inundation. In Marin County in particular, there are cases where neighboring fire stations are experiencing reductions in time accessibility as some road connections are cut off. In these cases, the delays can amount to 7 or 8 minutes. However, fewer similar cases can be found in other counties in the Bay Area.

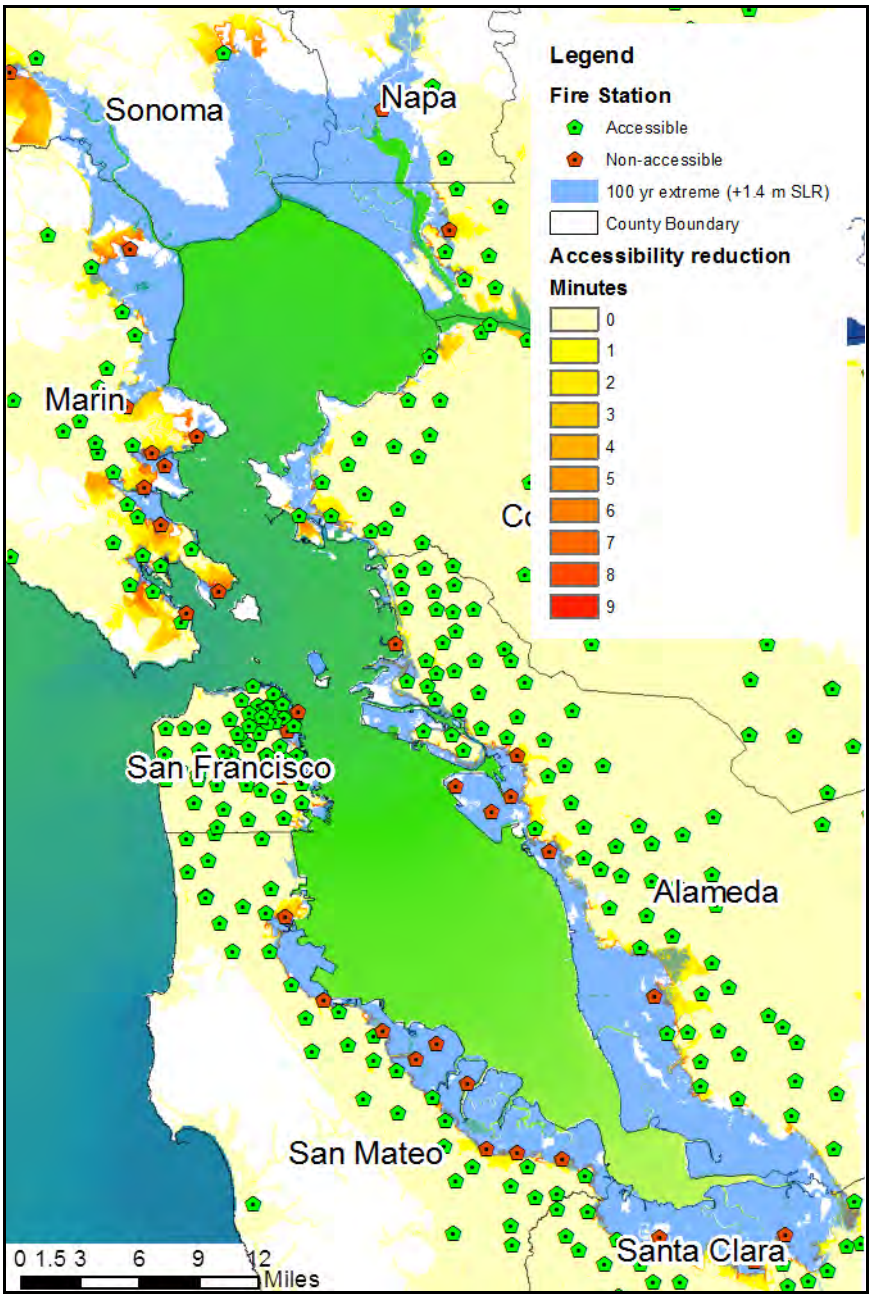

Figure 23. Time Reduction in Accessibility in First Responders under a 100-Year Storm Event in Combination with 1.4 m Sea-Level Rise.

3.3 Zonal Vulnerability of the Traffic Network

As a quantitative measure of regional vulnerability of the road network under potential inundation, we calculated the loss of accessibility by measuring the impact of travel time between nodes (intersections) of the major regional transportation system surrounding the San Francisco Bay. Figure 24 maps the travel time increments (measured as multiples of normal travel time) between intersections after a 100-year extreme event with different sea-level rise scenarios ((a) none or 0 m, (b) 0.5 m, (c) 1.0 m, and (d) 1.4 m).

For $PWL_{(0)}$ in Figure 24(a) node 19 in Marin county becomes inaccessible via major San Francisco Bay highways and access time between nodes 17 and 18 increases by a factor of 4–5 times. Of course it is rare for any node to become absolutely inaccessible. For example, we could expand our search network outside the nine-county region, where it would be possible for one to traverse a distant network to achieve topological connectivity, but it would be misleading and not practical for our purposes here. In such a metric, node 19 above would still be accessible, but relatively, it would appear extreme and essentially isolated.

For practical computational purposes, we limited the calculations to the nine-county San Francisco Bay region transportation network. Most of the north-south access time in the bay region increases by a factor of 1–2 times. For $PWL_{(0.5)}$ in Figure 24(b) we see a dramatic increase in access time east-west (as much as a factor of 11 times) as access to cross bay bridges begins to fail. In addition, node 21 in north San Mateo County is rendered inaccessible via major highways. North-south access time increases between 1–3 times. Figure 24(c) illustrates the results from $PWL_{(1.0)}$, which are not dramatically different from a $PWL_{(0.5)}$ save for an increase by a factor of 6–11 times in access time between nodes 15 and 18. Finally, at a $PWL_{(1.4)}$ nodes 17 and 20 join nodes 19 and 21 and are no longer accessible via major highways. In addition, there are some increased east-west access times ranging from 3 times to 4–5 times normal access in the south bay. In this final model, both Napa and Sonoma counties become isolated via major highways and access to Marin County is severely constrained.

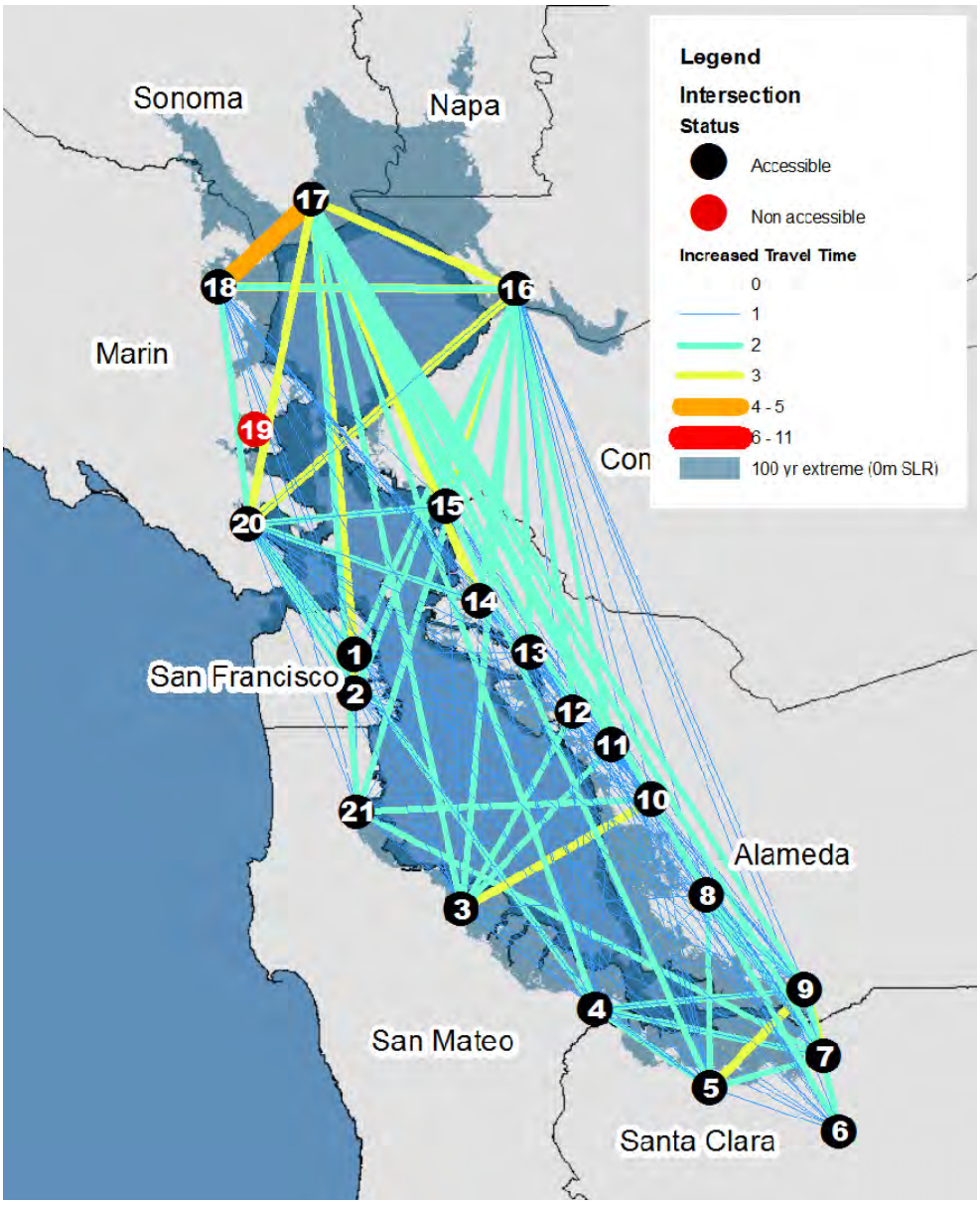
Legend
Intersection
Status
Accessible
Non accessible
Increased Travel Time
0
1
2
3
4 - 5
6 - 11
100 yr extreme (0m SLR)
Sonoma
Napa
Marin
Con
San Francisco
Alameda
San Mateo
Santa Clara
17
18
16
19
20
15
14
1
13
2
12
11
21
10
8
3
9
4
7
5
6

(a)

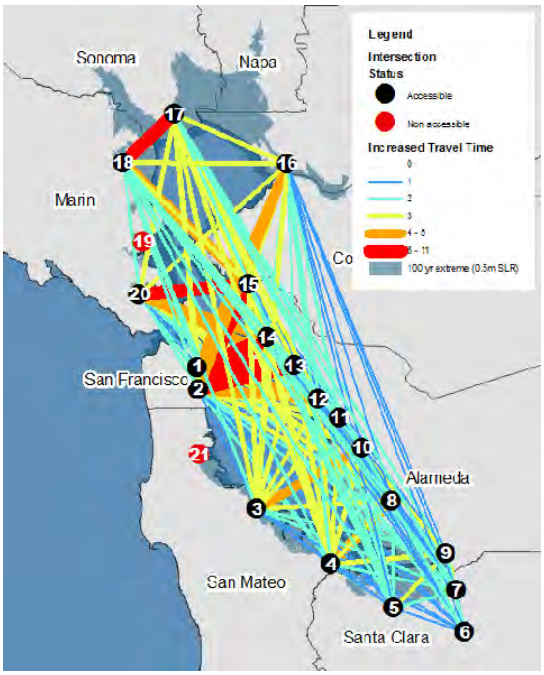

(b)

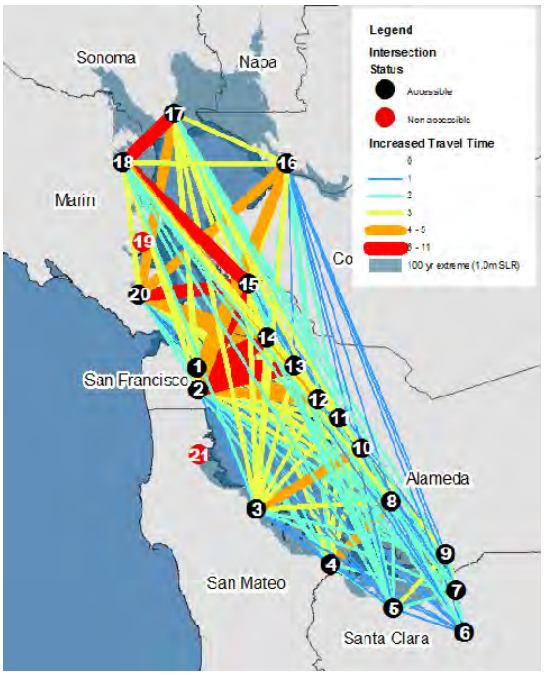

(c)

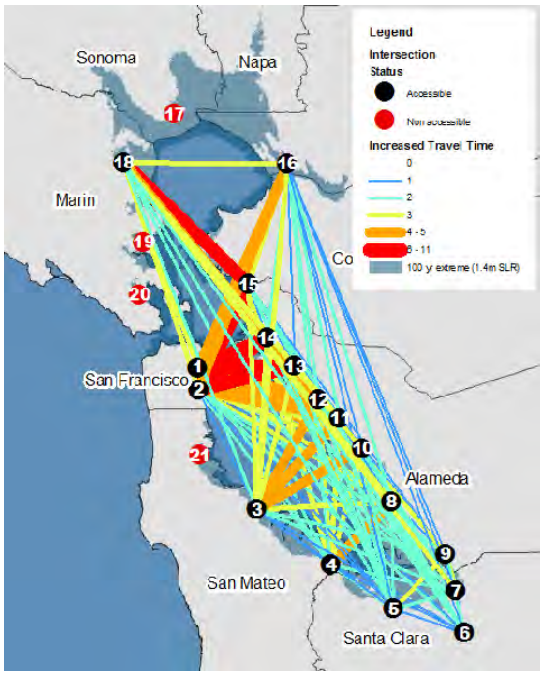

(d)

Figure 24. Increased Travel Time (as Multiples of Normal Travel Time) between Intersections after a 100-Year Extreme Event with Different Sea-Level Rise Scenarios. (An impressionistic graphic, due to the complexly of the connected graph). (a) None or 0 m, (b) 0.5 m, (c) 1.0 m, and (d) 1.4 m.

Figure 25(a-d) illustrates the greatest impact on individual links in the sample network by mapping the near neighbor accessibility. This figure essentially extracts and maps the increased access time (as multiples of normal travel times) to near neighbor nodes. We concluded that the

east-west impedance dominates the north-south impact, and the major regional network itself breaks in several locations as key nodes become inaccessible. We assume much of the regional system remains accessible via secondary roadways further inland and not adjacent to areas of inundation.

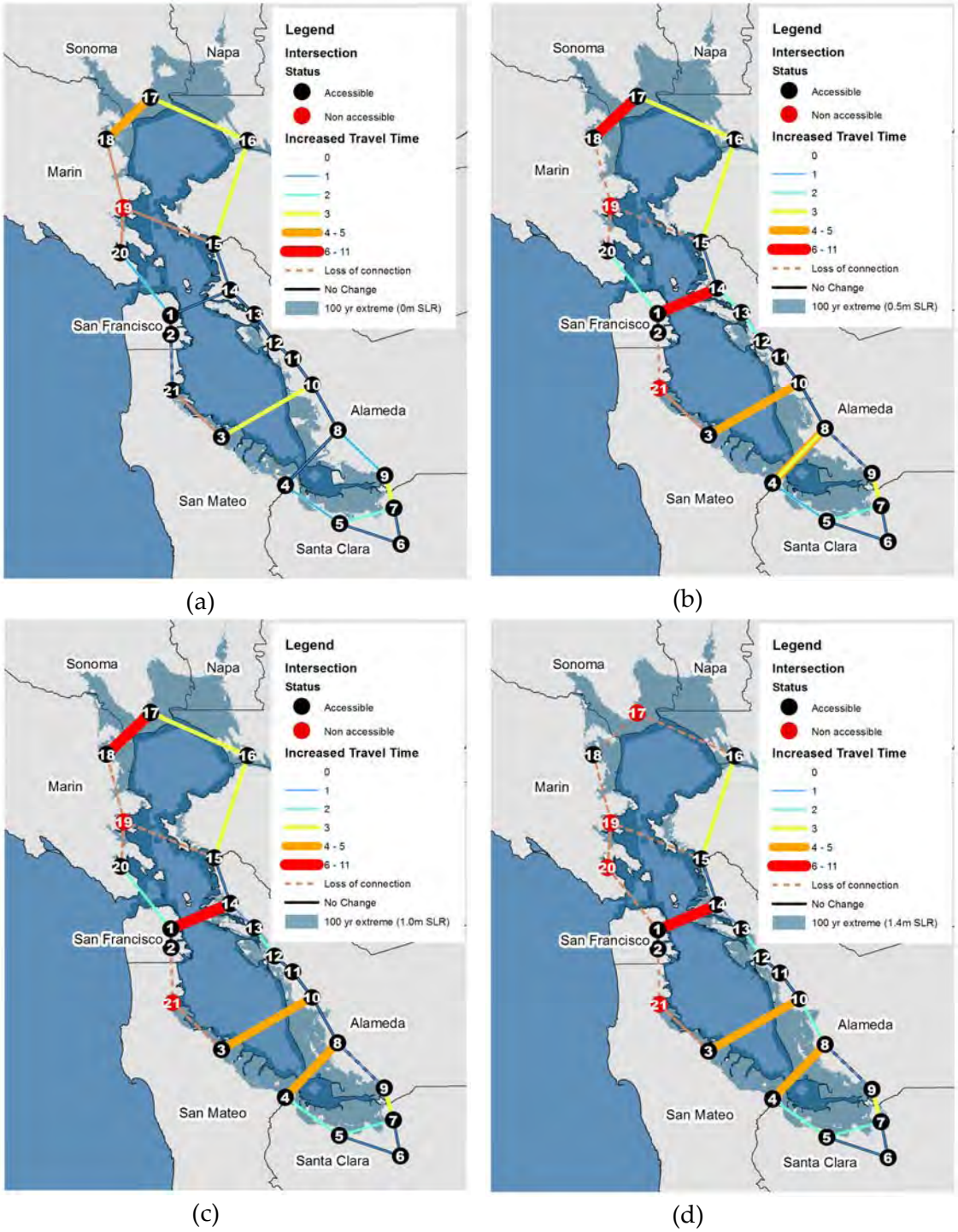

Figure 25. Increased Travel Time (as Multiples of Normal Travel Time) between Near-Neighbor Intersections after a 100-Year Extreme Event with Different Sea-Level Rise Scenarios. (a) None or 0 m, (b) 0.5 m, (c) 1.0 m, and (d) 1.4 m.

Figure 26 shows the annual average daily traffic, which ranges from 44,000 to over 200,000 vehicles per day for the nearest neighbor links on the regional transportation network.

Figure 26. Annual Average Daily Traffic Between Near-Neighbor Intersections under Current Conditions.

Figure 27 shows the traffic volume–weighted increment of travel distance under the disruption of a 100-year extreme event with different sea-level rise scenarios ((a) none or 0 m, (b) 0.5 m, (c) 1.0 m, and (d) 1.4 m). For $PWL_{(0)}$ in Figure 27(a) we see major disruptions in Marin and San Mateo counties and increased traffic volume on the Carquinez (between nodes 15 and 16) and the San Mateo (between nodes 3 and 10) bridges to accommodate the diverted traffic. For $PWL_{(0.5)}$ in Figure 27(b), the Bay Bridge experiences extremely high volumes. The network volumes are not significantly affected by further inundation.

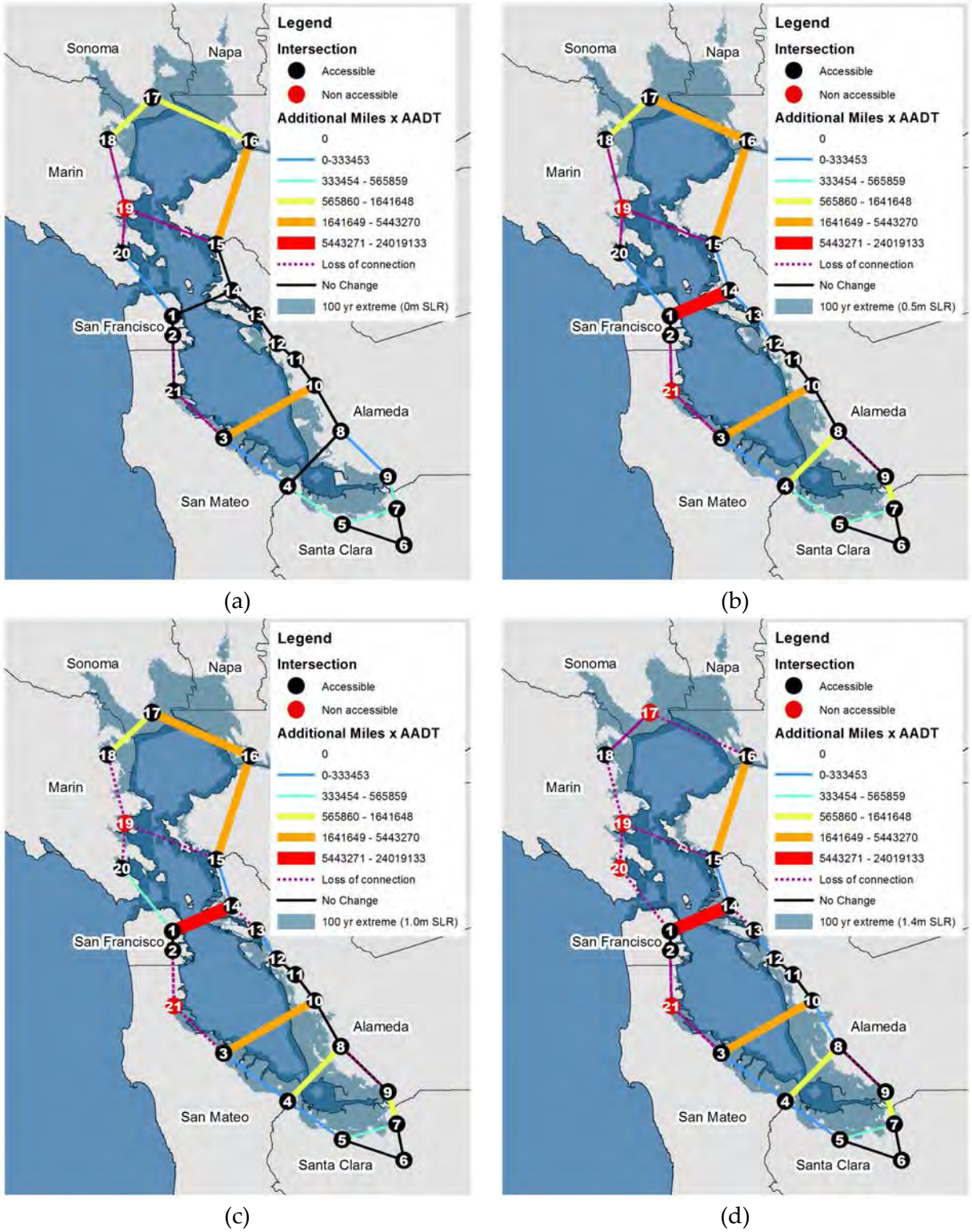

Figure 27. Traffic Volume–Weighted Increment of Travel Distance (Travel Distance Increments Multiplied by Traffic Volume) Between Nearest-Neighbor Intersections for the 100-Year Extreme Event with Different Sea-Level Rise Scenarios. (a) None or 0 m, (b) 0.5 m, (c) 1.0 m, and (d) 1.4 m.

Finally, we quantitatively measured the impact on accessibility to the hinterland from the major highway intersections, characterizing the first and last 20 minutes of an origin-destination journey. Figure 28 maps the baseline with dark green polygons representing the 5-minute travel time penetration into the hinterland, while light green and orange represent 10- and 15-minute travel times into the hinterland from the major traffic corridor intersections respectively. Finally red polygons represent the 20-minute travel extent.

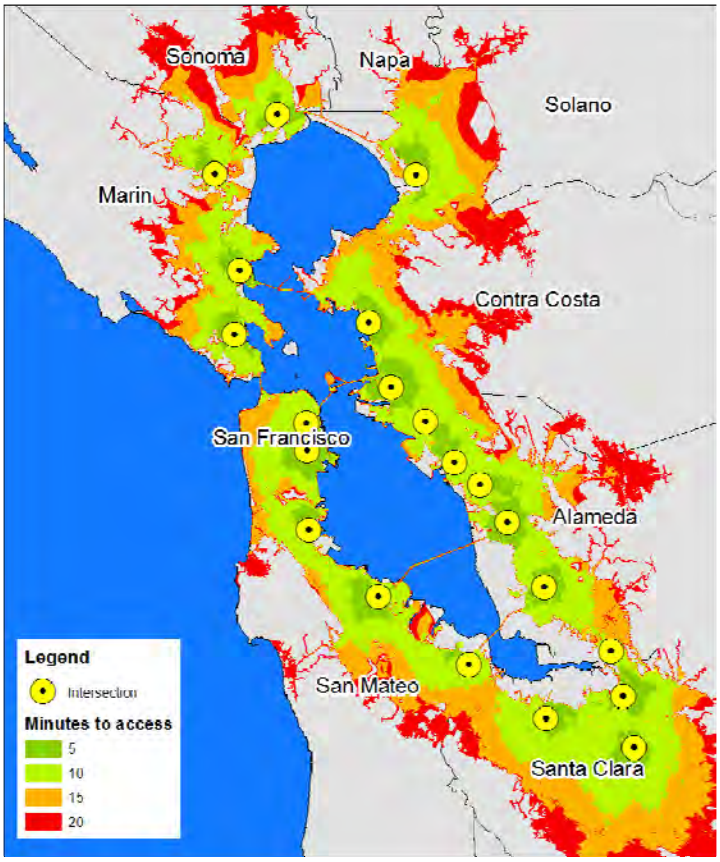

Figure 28. Hinterland Accessibility to Major Traffic Corridor Intersections.

Figures 29(a)–(d) show the impacts on hinterland accessibility to major traffic corridor intersections (major highway nodes). The results of our analysis show access into the hinterland in the North Bay is devastated by inundation. It begins for $PWL_{(0)}$ in Figure 29(a) and by the time of $PWL_{(1.4)}$ in Figure 29(d), the hinterland is unreachable from four major highway intersections. For the rest of the bay region, for the land that is not inundated, access to the major intersections is relatively stable.

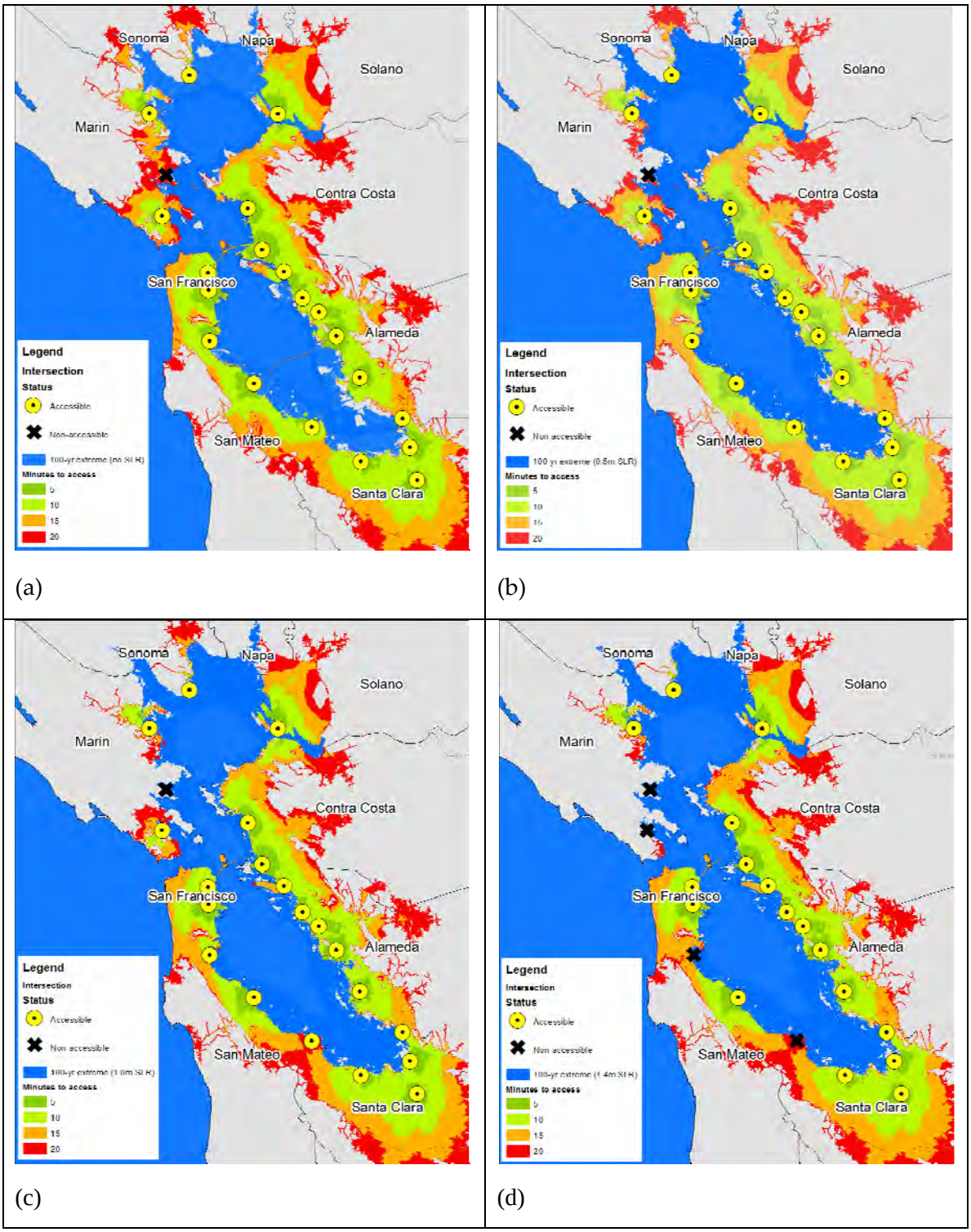

Figure 29. Impacts on Hinterland Accessibility to Major Traffic Corridor Intersections by a 100-Year Extreme Event with Different Sea-Level Rise Scenarios. (a) None or 0 m, (b) 0.5 m, (c) 1.0 m, and (d) 1.4 m.

Section 4: Discussion and Conclusions

The potential effects that climate change will have on the San Francisco Bay Area's shoreline and infrastructure have been previously reported on in Knowles (2009, 2010), Heberger et al. (2009), and BCDC (2009). This report adds to that literature base by reanalyzing the greater Bay Area using newly created surface models (DEMs), derived from the latest LiDAR, which has a finer resolution in the x, y, and z dimensions than was available in these earlier studies. This yields a better three-dimensional representation of the bare ground elevation profile of the Bay Area. In our research, we found that utilizing a DEM to determine water depth overestimates the amount of inundation area. When we used a DEM in combination with a water path algorithm, we saw a reduction in the amount of area indicated to be flooded under sea-level rise and 100-year flooding from an extreme storm event.

We created a digital surface model of infrastructure and buildings. DSMs contain information about not only the height of bare ground but also about the surface elevations of the objects on the ground. For example, in the case of raised bridges or highways, using a DEM only would falsely indicate the particular infrastructure as inundated. The elevated positions of such infrastructure can be determined with a DSM, thus avoiding this type of false positive inundations. Our results show that the overestimation of inundation using solely a DEM is greatest at the lowest inundation levels and the difference decreases with increasing inundation levels.

We chose to consider the joint effect of increases in sea level with 100-year extreme storm events on first responders. Because first responders are well distributed throughout the cities and counties, they are a good choice for study. When roads or highways are deemed impassable, we can study the increase in time for first responders to reach locations in their area of responsibility. We employed a constrained location-allocation model and measured the accessibility of first responders (supply) to households (demand) in a region demarcated by the first responders traveling along the shortest path to all households in the region. Using this model, we can largely capture local affects and for the two examples we provided (Richmond and north Santa Clara), the road topology is broken at $PWL_{(0.5)}$ or greater. Although we chose first responders, the method is universal and could serve to model the localized disruption in movement between any service and the population at large.

We employ a collection of major highway intersections as nodes in a trans-regional commuter network. These intersections are used in an origin-destination analysis looking at the impact on accessibility, as measured by increases in commuter time, that sea-level rise and 100-year extreme storm events have on trans-regional commuting. Using this model, we captured regional commute impacts and showed the east-west regional movement is impacted from 3 to as much as 11 times normal, while north-south impacts range from no impact to less than 3 times normal at $PWL_{(0.5)}$ – $PWL_{(1.4)}$. We also showed several critical nodes become orphaned at $PWL_{(1.4)}$. We weighted these major regional links with weights based on traffic volume, and mapped the greatest traffic flow impacts. The cross-Bay links disrupt the greatest volumes of traffic and prove to be critical components of the regional network.

We modeled and measured the accessibility into the hinterland from the major nodes along the trans-regional commuter network. Our results show that access into the hinterland in the North Bay is devastated by inundation and there are areas such as north San Mateo County where access to the major transportation road system is impacted. However, for the rest of the bay region, for the land that is not inundated itself, access to the major intersections is relatively stable.

Finally, extreme PWL will occur with increasing frequency as a result of higher mean sea level (Cayan et. al 2008 and Knowles 2010). This could result in greater stresses on levees currently protecting infrastructure. Figure 30 (from Knowles 2010) implies that by mid-century, today's 100-year extreme storm event with $SLR_{(0)}$ may become a one-year peak event with a 50 -cm SLR. In other words, in mid-century, when sea level has risen 50 cm, it takes a lesser storm event to create an impact equivalent to a 100-year peak event occurring today. Likewise, Cayan (2008) shows that when SLR rises to 0.80 m by 2100, the occurrence of extreme events increases from approximately one hourly event in one year to over 17 events in the last 30 years of the century.

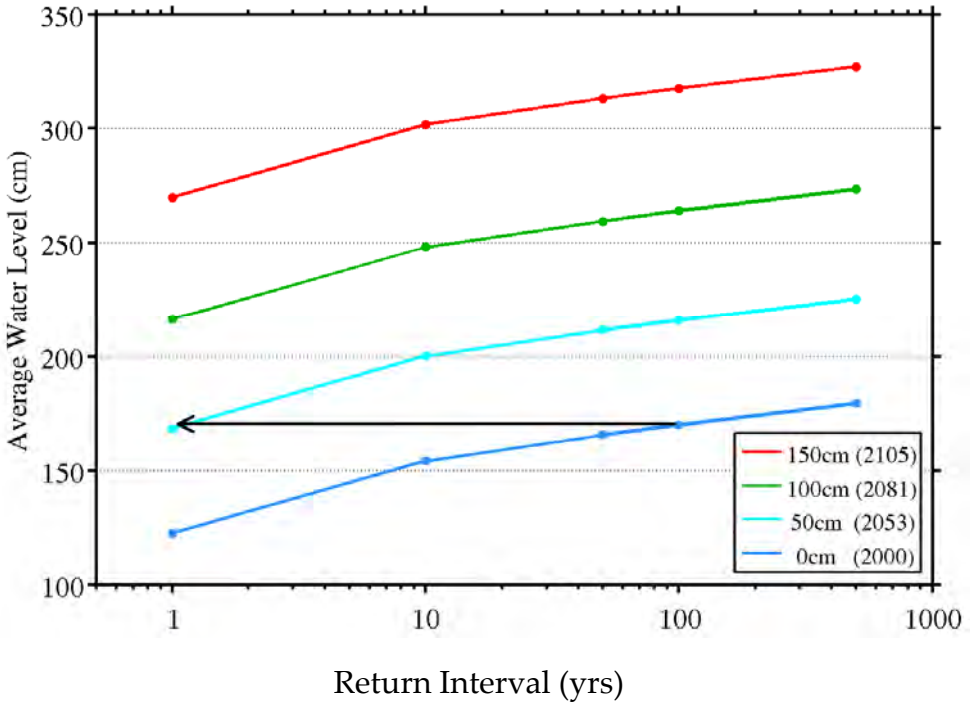

Source: Knowles (2010)

Figure 30. As Early as 2050, with Sea-Level Rise, the Water Level with a 1-Year Peak Event Could Equal Today's Water Level with 100-Year Peak Event.

References

Bay Area Council Economic Institute. 2008. Information about the Bay Area economy. Available at: http://www.bayeconfor.org.

BCDC (San Francisco Bay Conservation and Development Commission). 2009. *Living with a Rising Bay: Vulnerability and Adaptation in San Francisco Bay and on Its Shoreline.* April 7 2009. [Revised September 23 2011]. Available:http://www.bcdc.ca.gov/BPA/LivingWithRisingBay.pdf.

BCDC. 2011. *Adapting to Rising Tides. Transportation vulnerability and risk assessment pilot project.* Technical Report. 314 pgs. November 2011. Available: http://www.mtc.ca.gov/planning/climate/RisingTides-TechnicalReport.pdf

Berdica, K. 2002. "An introduction to road vulnerability: What has been done is done and should be done." *Transport Policy* 9:117–127.

Bromirski, P. D., R. E. Flick, and D. R. Cayan. 2003. "Storminess variability along the California coast: 1858–2000." *J. Clim*. 16: 982–993.

Bromirski, P. D., D. R. Cayan, N. Graham, R. E. Flick and M. Tyree (Scripps Institution of Oceanography). 2012. Coastal Flooding Potential-Projections 2000–2100. California Energy Commission. CEC-500-2012-011.

California Department of Transportation. 2009. Vulnerability of Transportation Systems to Sea-level rise (Preliminary Assessment).

Cayan, D., P. Bromirski, K. Hayhoe, M. Tyree, M. Dettinger and R. Flick. 2008. "Climate Change projections of sea level extremes along the California coast." *Climatic Change* 87(Suppl 1):S57–S73.

Cayan, D., M. Tyree, M. Dettinger, H. Hidalgo, T. Das, E. Maurer, P. Bromirski, N. Graham, and R. Flick. 2009. Climate change scenarios and sea-level rise estimates for the California 2009 climate change scenario assessment. California Climate Change Center. CEC-500-2009-014-F, California Energy Commission, PIER Energy-Related Environmental Research. Available: http://www.energy.ca.gov/2009publications/CEC-500-2009-014/CEC-500-2009-014-D.PDF.

Chang, H., M. Lafrenz, I. W. Jung, M. Figliozzi, D. Platman, and C. Pederso. 2010. "Potential Impacts of Climate Change on Flood-Induced Travel Disruptions: A Case Study of Portland, Oregon, USA." *Annals of the Association of American Geographers* 100: 938–939.

Cheng, R. T., and J. W. Gartner. 1984. *Tides, tidal and residual currents in San Francisco Bay California - results of measurements, 1979–1980.* U.S. Geological Survey Water-Resources Investigations Report No. 84-4339.

D'Este, G. 2003. Network vulnerability: An approach to reliability analysis at the level of national strategic transport networks. Network reliability of transport: proceedings of the 1st International Symposium on Transportation Network Reliability. 9–30.

Dewberry. 2011a. Project report for the USGS San Francisco Coastal LiDAR – ARRA LiDAR. Prepared for USGS. March 4 2011. 137 pgs.

Dewberry. 2011b. LiDAR quality assurance (QA)report. San Francisco Bay LiDAR Project. Submitted to: NOAA Coastal Service Center. April 21 2011. 40 pgs.

ESRI. 2009. ArcGIS 9.3.1, Environmental Systems Research Institute, Redlands, California.

Flick, R. E. 1998. "Comparison of California tides, storm surges, and mean sea level during the El Niño winters of 1982–1983 and 1997–1998." *Shore & Beach* 66(3):7–11.

Flick, R. E., J. F. Murray, and L. C. Ewing. 2003. "Trends in United States Tidal Datum Statistics and Tide Range." *J. Waterway, Port, Coastal and Ocean Eng., Amer. Soc. Civil Eng*. 129 (4): 155–164.

Ford, J. D. and B. Smit. 2004. "A framework for assessing the vulnerability of communities in the Canadian Arctic to risks associated with climate change." *Arctic* 57: 389–400.

Heberger, M., H. Cooley, P. Herrera, P. Gleick, and E. Moore. 2009. The impacts of sea-level rise on the California coast. California Energy Commission Report No. CEC-500-2009-024-F.

Holmgren, Å. 2004. Vulnerability analysis of electric power delivery networks (Licentiate Thesis. Land and Water Resource Engineering, The Royal Institute of Technology. Stockholm. ISSN). 32 pgs.

Husdal, J. 2004. Reliability and vulnerability versus cost and benefits. In *Proceedings of the Second International Symposium on Transportation Network Reliability (INSTR)* (Christchurch, New Zealand), 182–188.

IPCC. 2001. Climate Change 2001: Impacts, Adaptation, and Vulnerability. Contribution of Working Group II to the Third Assessment Report of the Intergrovernmental Panel on Climate Change. Cambridge University Press: Cambridge, UK.

IPCC. 2007. Climate Change 2007: Impacts, Adaptation, and Vulnerability. Contribution of Working Group II to the Fourth Assessment Report of the Intergovernmental Panel on Climate Change. Cambridge University Press: Cambridge, UK.

Jenelius, E., T. Petersen, and L. G. Mattsson. 2006. "Importance and exposure in road network vulnerability analysis." *Transportation Research Part A: Policy and Practice* 40: 537–560.

Kahrl, F., and D. Roland-Holst. 2008. *California climate risk and response.* University of California, Berkeley. 127 pgs.

Keim, B., T. W Doyle, V. R. Burkett, I. Van Heerden, S. A. Binselam, M. F. Wehner, C. Tebaldi, T. G. Houston, and T. G. Beagan. 2008. How is the Gulf Coast Climate Changing? Impacts of Climate Change and Variability on Transportation Systems and Infrastructure: Gulf Coast Study, Phase I. U.S. Climate Change Science Program.

Knowles, N. 2008. Potential Inundation Due to Rising Sea Levels in the San Francisco Bay Region. A report from the California Climate Change Center, sponsored by the California

Energy Commission and the California Environmental Protection Agency, Sacramento, California. CEC-500-2009-023-F.

Knowles, N. 2009. Potential Inundation Due to Rising Sea Levels in the San Francisco Bay Region. California Climate Change Center. CEC-500-2009-023-F, California Energy Commission, PIER Energy-Related Environmental Research. Available: http://www.energy.ca.gov/2009publications/CEC-500-2009-023/CEC-500-2009-023-D.PDF.

Knowles, N. 2010. "Potential Inundation Due to Rising Sea Levels in the San Francisco Bay Region." *San Francisco Estuary and Watershed Science* 8(1): 1–19. Available: http://escholarship.org/uc/item/8ck5h3qn.

Laurentius, G. 1994. The vulnerability of the city. Planning a High Resilience Society. Swedish Agency for Civil Emergency and Planning (OCB) and Umea Universitet. Geographical Reports 11.

Miller, H. 1999. "Measuring Space-time accessibility benefits within transportation networks: Basic Theory and Computational Procedures." *Journal of Planning Literature* 40(6): 491–506.

Moss, R. E. S., and J. M. Eller. 2007. Estimating the Probability of Failure and Associated Risk of the California Bay Delta Levee System. 10 pgs.

MTC (Metropolitan Transportation Commission). 2004. *Regional Goods Movement Study for the San Francisco Bay Area.* Final Summary Report. 21 pgs.

MTC. 2007. *San Francisco Bay Area Regional Rail Plan.* Final Report. 27 pgs.

MTC and Caltrans - D4. 2008. Bay Area Transportation: State of the System 2008 (Oakland, California). Available at: http://www.mtc.ca.gov/library/state_of_the_system/index_2003-07.htm.

MTC. 2009. *Change in motion, Transportation 2035 Plan for the San Francisco Bay Area*. 142 pgs.

MTC, BCDC, and ABAG (Association of Bay Area Governments). 2011. *Regional Airport System Planning Analysis. 2011 Update. Volume 2: Major Reports.* 378 pgs.

Nakicenovic, N., J. Alcamo, G. Davis, B. de Vries, J. Fenhann, S. Gaffin, K. Gregory, A. Grubler, T. Y. Jung, T. Kram, et al. 2000. *Special report on emissions scenarios: A special report of Working Group III of the Intergovernmental Panel on Climate Change.* Pacific Northwest National Laboratory, Richland, Washington, Environmental Molecular Sciences Laboratory. 599 pgs.

National Research Council (NRC). 2008. Potential Impacts of Climate Change on U.S. Transportation. Transportation Research Board Special Report 290. Transportation Research Board, Washington, D.C. 218 pgs.

Nicholls, R. J., F. M. Hoozemans, and M. Marchand. 1999. "Increasing flood risk and wetland losses due to global sea-level rise: Regional and global analyses." *Global Environmental Change* 9: S69–S87.

Peterson, T. C., M. McGuirk, T. G. Houston, A. H. Horvitz, and M. F. Wehner. 2008. Climate Variability and Change with Implications for Transportation Climate Variability and Change with Implications for Transportation.

Radke, J., and M. Lan. 2000. "Spatial Decompositions, Modeling and Mapping Service Regions to Predict Access to Social Programs." *Geographic Information Sciences* 6(2): 105–112.

Rahmstorf, S. 2007. "A Semi-Empirical Approach to Projecting Future Sea-Level Rise." *Science* 315(5810): 368.

Ryan H., H. Gibbons, J. W. Hendley, and P. Stauffer. 1999. El Niño sea-level rise wreaks havoc in California's San Francisco Bay Region. USGS Fact Sheet 175–99. Available: http://pubs.usgs.gov/fs/1999/fs175-99/.

Santos, B., A. Antunes, and E. Miller. 2010. "Interurban Road Network Planning Model with Accessibility and Robustness Objectives." *Transportation Planning Technology* 33(3): 297–313.

Sohn, J. 2006. "Evaluating the significance of highway network links under the flood damage: An accessibility approach." *Transportation Research Part A: Policy and Practice* 40: 491–506.

Suarez, P., W. Anderson, V. Mahal, and T. Lakshmanan. 2005. "Impacts of flooding and climate change on urban transportation: A systemwide performance assessment of the Boston Metro Area." *Transportation Research Part D: Transport and Environment* 10: 231–244.

Taylor, M. A., and G. M. D'Este. 2004. Critical infrastructure and transport network vulnerability: Developing a method for diagnosis and assessment. Proceedings of the Second International Symposium on Transportation Network Reliability (INSTR) (Christchurch, New Zealand), pp. 96–102.

Taylor, M. A. P., S. V. C. Sekhar, and G. M. D'Este. 2006. "Application of accessibility based methods for vulnerability analysis of strategic road networks." *Networks and Spatial Economics* 6: 267–291.

Titus, J. 2002. Does Sea-level Rise Matter to Transportation Along the Atlantic Coast? Proceeding of the Potential Impacts of Climate Change on Transportation, October 2002, Washington, D.C., 1–16.

Transportation Research Board. 2008. Potential impacts of climate change on US transportation. TRB Special Report 290. Washington, D.C.

United States Army Corps of Engineers. 1984. *San Francisco Bay Tidal Stage vs. Frequency Study.* San Francisco, California. October. 23 pgs.

URS. 2009. Delta Risk Management Strategy: Section 13, Risk Analysis 2005 Base Year Results. Prepared for the California Department of Water Resources.

Vermeer, M., and S. Rahmstorf. 2009. "Global sea level linked to global temperature." *Proc. Natl. Acad. Sci.* 106: 21527–21532.

Wehr, A., and U. Lohr. 1999. "Airborne laser scanning–an introduction and overview." *ISPRS Journal of Photogrammetry and Remote Sensing* 54: 68–82.

Wilkinson, R., K. Clarke, J. Reichman, and J. Dozier. 2002. *Preparing for a changing climate: The potential consequences of climate variability and change for California.* Report for the U.S. Global Change Research Program. 431 pgs.

Zetler, B. D., and R. E. Flick. 1985. "Predicted Extreme High Tides for California, 1983–2000." *J. Waterway Port, Coastal and Ocean Eng., Amer. Soc. Civil Eng.* 111(4): 758–765.

Glossary

A1B	mid-range emission scenario
AADT	Annual Average Daily Traffic
ABAG	Association of Bay Area Governments
B1	low-emission scenario
BART	Bay Area Rapid Transit
BCDC	Bay Conservation and Development Commission
CCLP	California Costal LiDAR Project
CCSM3	Community Climate System Model
CLICK	Center for LIDAR Information Coordination and Knowledge
DEM	digital elevation model
DOT	California Department of Transportation
DRMS	Delta Risk Management Strategy
DSM	digital surface model
ESE100	100-year extreme storm event
ESRI	Environmental Systems Research Institute
FVA	Fundamental Vertical Accuracy
GCM	Global Climate Model
GIS	Geographic Information System
IPCC	Intergovernmental Panel on Climate Change
LiDAR	Light Detection and Ranging
MHHW	Mean Higher High Water
MHW	Mean High Water
MLLW	Mean Lower Low Water
MLW	Mean Low Water
MSL	Mean Sea Level
MTC	Metropolitan Transportation Commission
MTL	Mean Tide Level
MUNI	Municipal Transportation Agency
NAD83	Universal Transverse Mercator projection
NAVD88	North American Vertical Datum of 1988
NED	National Elevation Dataset
NOAA	National Oceanic and Atmospheric Administration
OAK	Oakland International Airport
PIER	Public Interest Energy Research
PWL	Peak Water Level
$PWL_{(0)}$	no sea-level rise
RD&D	Research, Development, and Demonstration
SFO	San Francisco International Airport
SJC	San Jose International Airport

SLR	sea-level rise
SRES	Special Report on Emissions Scenarios
TCA	Terminal Control Areas
TEUs	Twenty-foot Equivalents
USGS	U.S. Geological Survey
UTM	Universal Transverse Mercator